Design, Development, and Evaluation of a Soft-Inflatable Exosuit for Lower Limb

Assistance

by

Saivimal Sridar

A Dissertation Presented in Partial Fulfillment
of the Requirements for the Degree
Doctor of Philosophy

Approved March 2020 by the
Graduate Supervisory Committee:

Wenlong Zhang, Chair
Thomas Sugar
Thurmon Lockhart

ARIZONA STATE UNIVERSITY

May 2020

ABSTRACT

Traditionally, wearable exoskeletons for gait assistance have addressed the issue of high power requirement of providing support during walking. However, exoskeletons often are bulky, and suffer from misalignment of joints between the robot and the user. Soft robots in recent work have shown the ability to provide a high degree of compliance with a light weight and lower cost. This work presents the design, control, and evaluation of a soft inflatable exosuit to assist knee extension. First, the design of novel soft inflatable actuators of I cross-section and their application in the soft inflatable exosuit is presented. The actuators are applied to a soft and lightweight garment interface to assist in knee extension during the swing phase demonstrating reduced muscle activity for the quadriceps. Second, the control of the soft exosuit is presented with the introduction of a knee angle measurement system and smart shoe insole sensors. A new control method using human joint stiffness models as well as actuator models is developed. The new control method is evaluated with three users and a reduction in the sEMG activity of the quadriceps is observed with an increase in the activity of the hamstrings. Third, an improved version of the exosuit and a controller to assist knee extension in swing phase and initial stance are presented. The exosuit is applied to seven healthy and three impaired participants. Kinematics, muscle activity and gait compensations are studied. Reduced muscle activity for the quadriceps is seen in healthy participants with reduced execution times for functional activities such as timed up-and-go as well as sit-to-stand transitions in impaired participants. Finally, an untethered version of the soft exosuit using inflatable actuator composites and a portable pneumatic source are presented. Finite element models for the composites and inflatable actuators are generated and the actuators are characterized for performance. The design of a portable source for the exosuit is also presented. The inflatable actuator composites and the portable source

are implemented in a portable exosuit system which demonstrated a reduction in the Vastus Lateralis activity during incline walking for three participants. Overall, this work investigated the feasibility of several versions of the soft exosuit for gait assistance.

ACKNOWLEDGMENTS

TABLE OF CONTENTS

LIST OF TABLES

LIST OF FIGURES

Chapter 1

INTRODUCTION

There are several issues such as physical disabilities affecting a large population all over the world. Stroke is regarded as one of the leading causes of disabilities in the world affecting a large populace [1]. Common effects of stroke are paralysis of limbs and loss of motor function in the victim with severe cases leading to death. The areas of the human body affected by stroke can include upper and lower extremities hence affecting daily activities such as walking. Stroke survivors often require physical rehabilitation to restore function of their affected limbs. The number of people affected by stroke exceeds 795,000 only in the United States as of 2011 with projected increase in the number of stroke incidences[2].

The loss of muscle function and control in stroke survivors can be attributed to weakness and spasticity [3, 4]. Looking at lower body in particular, muscular weakness in the quadriceps, hamstrings, and calf muscles has been reported[5]. The loss of function in the aforementioned muscle groups can lead to the inability to walk in a healthy manner. To overcome the weakness in strength and muscle control, individuals adopt compensatory walking patterns that lead to a higher energy expenditure during walking as well as social stigma[6]. Therefore, physical rehabilitation plays a key role in post stroke recovery.

Furthermore, the number of people over the age of sixty is expected to double by the year 2050 [7]. The aged people tend to lose muscle strength and also to develop physical ailments such as arthritis and hip dysplasia which can affect them in activities of daily living. Therefore, to support the aging population there is a need for caregivers to help in performing daily activities. Further, some aging adults also

undergo physical rehabilitation in order to build strength and muscle control.

The younger population working in manual material handling often carry and move large weights on a daily basis. This puts significant loads on the knees, hips, and lower back of the person performing the task. In a recent survey, more than 42% of lower-body injuries in the physical work force are caused by over-straining and exertion. Work-related injuries lead to reduced quality of life, loss of pay for workers and increased costs of operation for the industry. Long-term ramifications of these musculoskeletal injuries for workers generally tends to be chronic problems such as slipped disks which significantly affects their life and livelihood.

Commonly used equipment in the industry involves the use of personal protective equipment(PPE) such as knee pads and steel-toed shoes which only provide protection from external sources of injuries and do not aid with strain related injuries. Additionally, workers may opt for commercially available knee and lumbar support braces to allow for alleviation of pressure loads but no studies showing the efficacy of such braces have been performed.

The increase in the number of physical disabilities and the need for physical rehabilitation has led to an increased load on physical therapists [9]. Therefore, the use for robotics in physical rehabilitation has increased drastically over the last few decades. Motor relearning in stroke therapy includes repetitive tasks performed over a period of time which leads to the re-wiring of neural pathways. The use of robots to assist in the repetitive tasks is shown to aid in physical therapy with the supervision of therapist[10, 11].

Due to shortage of caregivers and clinicians [8], aging population could potentially benefit from the use of wearable robots in order to perform strenuous tasks such as walking up stairs and sit to stand transfers. Also, the use of wearable robots could aid in the prevention of accidents such as slips and falls that lead to further complications.

In manual material handling, wearable robots can be used as a preventative measure to reduce musculoskeletal injuries. Recent studies with back exoskeletons have shown reduced muscle activity and metabolic costs during lifting. Offloading significant loads from carrying heavy packages and boxes can potentially lead to better long term benefits for the workers as well as the industry.

1.1   Literature Review

1.1.1   Exoskeletons

Exoskeleton robots have potential to provide assistance for various tasks such as physical rehabilitation as well as manual material handling. Commonly used actu-

Rewalk	Indego	Ekso Bionics	Rex Bionics	B-Temia	Fourier X1	SuitX

Figure 1.1 Commercially Available Exoskeletons for Gait Rehabilitation.

ators for rigid wearable robots include motors and pneumatic cylinders [12]. These actuators are energy efficient and are capable of generating large force outputs with the cost of of higher weight. Exoskeletons in rehabilitation[13, 14] are highly effective in providing assisted guidance to the users aiding in faster recovery as shown by various studies[15, 16, 17]. The use of exoskeletons in physical rehabilitation in conjunction with traditional therapy has demonstrated faster motor relearning and gait retention as compared to just physical therapy[18]. Also, there have been several commercially available exoskeletons that are tailored towards physical rehabilitation with some depicted in Fig. 1.1.

Furthermore, several studies and surveys have been performed highlighting the need for wearable exoskeletons and wearable robots [19, 20]. Work on exoskeletons and wearable systems for aging population in order to ease exertion as well as avoid injuries have also been investigated [21]. The use of exoskeletons for problems such as sit-to-stand transfers [22] have been demonstrated.

Work on utilizing exoskeletons for assisting the back and lower-body during lifting have also been demonstrated by several groups [23, 24, 25]. These exoskeletons have shown effectiveness in reducing the muscle effort during lifting while maintaining posture. Several commercially available exoskeletons for aiding in lifting are currently being implemented on shop floors [PAEXO etc.].

Although these exoskeletons have demonstrated efficacy of use in several afore-mentioned applications, several issues still persist. The downside to rigid exoskeletons is the higher weight and bulk which makes them unsuitable for use in small or in-home settings. Also, exoskeletons are usually affected by joint mismatch where the human and the robot joint center are misaligned, leading to user discomfort [26]. Also, exoskeleton robots are typically expensive therefore, are not available to day to day users making them unsuitable for frequent use in a small setting.

1.1.2 Soft Actuators for wearable applications

Soft robotics is classified as a subset of robotics that makes use of unconventional means of actuation and sensing such as elastomers, fabrics, and cable driven mechanisms as opposed to rigid manipulators[27, 28, 29]. The primary advantage of soft robotics over traditional means of robotics is the compliance it offers aiding in the human-robot interaction with high power to weight ratio and relatively inexpensive fabrication cost.

Soft robotics can predominantly separated into - Elastomeric actuators, cable
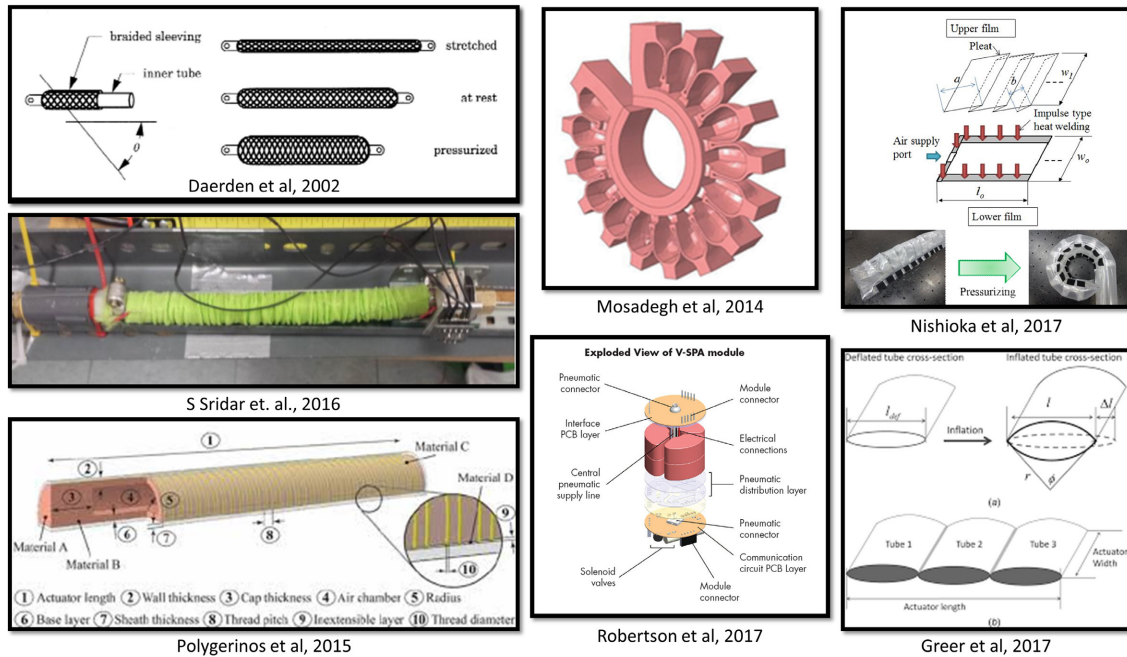
Figure 1.2 Soft Actuators of Elastomeric and Film-Based Actuators.

driven mechanisms, fabric/film based actuators, shape memory alloys, electro-active polymers, and shape morphing polymers [30]. Although each type of actuator provides its own set of advantages, the scope of this work is limited to wearable robots for use in physical rehabilitation. Therefore, the major focus of this study will be restricted to elastomeric, fabric/film based, and cable driven mechanisms which have been utilized in wearable systems.

The elastomeric actuators comprise of a set of actuators that are fabricated using elastic and hyper-elastic materials that are capable of stretching in excess 2-3 times their original length. The actuation methods for the elastomeric actuators include pneumatic, hydraulic, and electro-active means. The pneumatic artificial muscle (PAM) [31] is considered as one of the most popular elastomer-based soft actuator . Some other elastomeric actuators include fiber-reinforced actuators(FRAs)[32], rPAMs[33], and HydroMuscle[34] that elongate upon application of internal pressure.

5

Further, work on electro-active silicone polymer material for use in elastomeric actuators has been demonstrated in [35].

Fabric or film based actuators involve thin films that are either individually actuated or bonded in layers to provide actuation through pneumatic, hydraulic, or electro-activation. Common fabric/film based actuators involve peano actuaors[36] and ELSA[37]. The cable driven mechanisms is a soft-means of actuation that requires a prime mover such as a motor to actuate the cables[38]. Overall, the actuator itself is not soft in nature but the method of actuation is considered soft owing to the compliance of the cables.

1.1.3 Soft Wearable Robots for lower body

Soft wearable robots can be classified into rehabilitative and assistive devices according to their application. The goal of rehabilitative devices is to provide targeted assistance to a body part that lacks the strength to perform a given task. Whereas in assistive devices, the aim is to augment the capabilities of the user by providing assistance and improving performance of executing a certain task.

When designing soft wearable robots, there are several factors that need to be taken into consideration. The external part of the human body itself is soft in nature due to the layer of the tissues and skin covering the body. Therefore, mounting wearable devices is challenging. As opposed to exoskeleton robots which have a structure, soft robots are entirely comprised of compliant materials. Hence, identifying anchor points on the human body is critical so that the assistance provided to the body through the wearable robot does not affect the user unintentionally [39].

The soft actuators mentioned in Section 1.1.2 have been applied to a variety of wearable robots for both human augmentation as well as physical rehabilitation. The application of soft actuators in wearable devices has been demonstrated for both up-

6
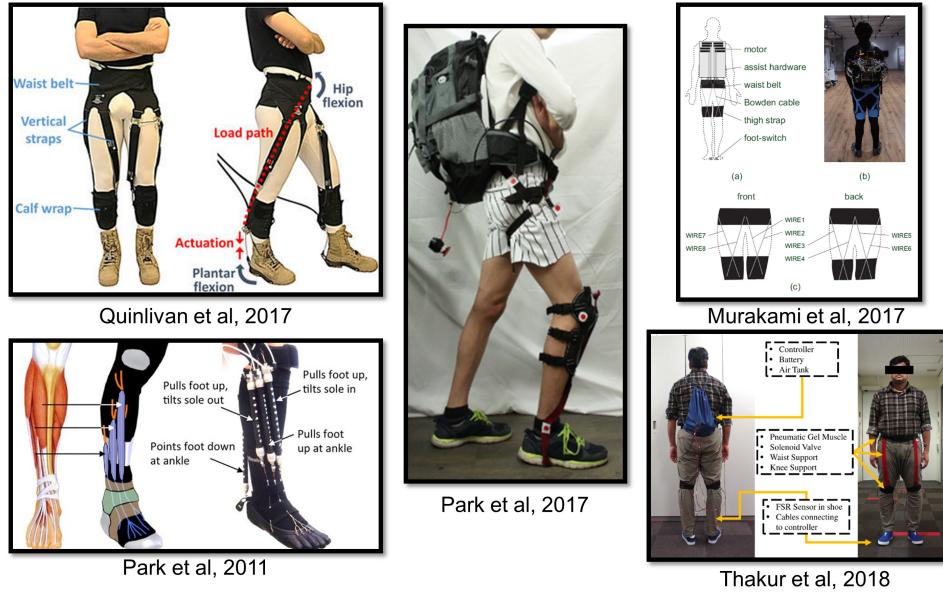
Figure 1.3 Soft Wearable Devices for Lower Limb Utilizing Cable Driven Mechanisms and Elastomeric Actuators.

per and lower limb assistance. Some of the most well known soft-wearable robots are the soft exosuit from the Harvard Bio-design group[40, 41, 42]. The application of elastomeric actuators as well as cable driven mechanisms has been demonstrated through rigorous participant testing and evaluation. Other soft-wearable devices involve the soft ankle foot orthotic from Carnegie Mellon University[43], Panasonic cross-wire suit[44], and Augment Walking Suit from Hiroshima University[45].

Prior work has demonstrated the use of fabric/film based actuators in soft robots for the upper body [46, 47, 48]. Most of the prior work for soft-wearable robots for the lower body has focused on cable driven or elastomeric actuators but very few groups have explored the use of fabric/film based actuators. There has been significant development in the wearable systems utilizing fabric-based actuators for the upper limbs[49, 50] but there is a significant gap in the development of fabric/film based wearable robots for the lower body[51, 52]. This work will focus on the design of a soft-wearable robot utilizing fabric and film based actuators.

7
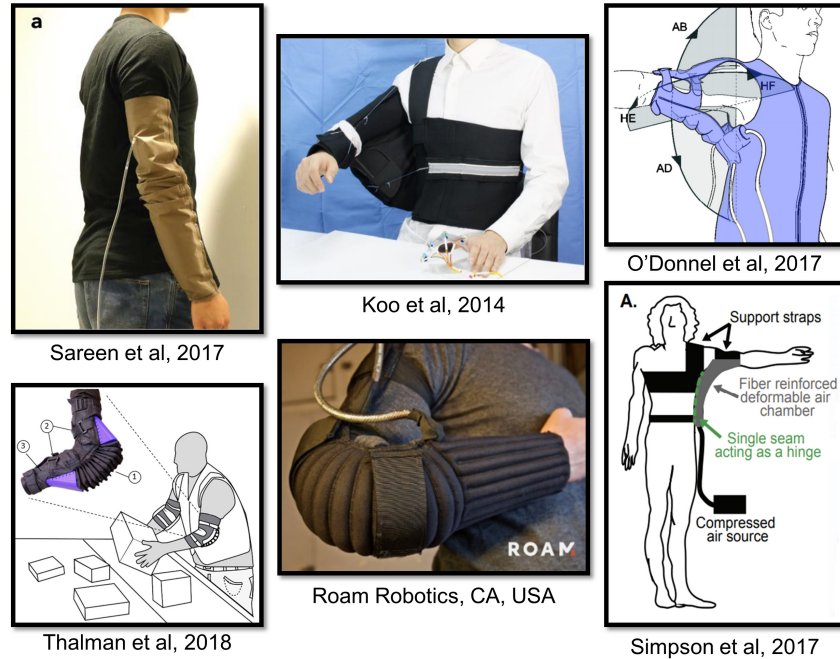
Figure 1.4 Soft Wearable Devices for Upper Limb Utilizing Fabric/Film Based Actuators.

1.2 Organization

This work focuses on the design and evaluation of a soft-inflatable exosuit to assist knee extension using inflatable actuators and demonstrate application of the exouit on healthy and impaired participants for physical augmentation and rehabilitation. This dissertation is organized as follows:

Chapter 2: This chapter presents the design of a soft-inflatable exosuit system which utilizes heat-sealed inflatable beams fabricated using thermoplastic polyurethane. The biomechanics of walking pertaining to the knee joint are studied and inflatable actuators of I and O cross-sections are compared. The design of the soft-inflatable exosuit using a neoprene knee sleeve, hook-and-loop straps, and inflatable actuators of I cross-section is presented. The exosuit is used to provide assistance to the knee extension during swing phase of walking and applied to one healthy test participant examining Vastus Lateralis muscle activity.

Chapter 3: Detailed characterization of the soft-inflatable actuators along with a stiffness control method for the soft-inflatable exosuit is presented. The soft exosuit is integrated with smart shoe insole sensors and inertial measurement units for gait phase and knee angle information feedback. The quasi-stiffness of the knee joint during the gait cycle is studied and soft-inflatable actuators are characterized for their stiffness with increasing internal pressure. A high level controller taking into account knee stiffness, actuator stiffness, and knee angle as feedback is developed. A low level controller to track the actuator pressure using solenoid valves is also designed. The soft-inflatable exosuit is applied to 3 healthy participants studying muscle activity of the quadriceps and hamstrings.

Chapter 4: The soft inflatable exosuit is applied to seven healthy and three impaired test participants providing knee extension assistance to the swing phase. Surface electromyographic activity of the quadriceps and hamstrings in healthy participants was examined, demonstrating reduced muscle activity. Furthermore, all impaired participants walked with smaller knee angles at heel strike with shorter step length and step time for treadmill walking. The compensatory gait patterns for the three participants were non-conclusive with a reduced timed up-and-go completion.

Chapter 5: To improve the portability of inflatable exosuits, low-volume inflatable actuator composites and a portable pneumatic source were designed. Finite element models for the inflatable actuators comparing the deflection of the previously designed fabric beams and composites were generated. The actuator was characterized for force output, hysteresis, and inflation speeds. The portable system was designed to generate both high flows and pressure output. A soft exosuit was fabricated using the inflatable composites and integrated with the portable source and smart shoe insole sensors. The portable exosuit was tested with three healthy test participants demonstrating reduction in muscle effort for the Vastus Lateralis during incline walking.

9

Chapter 6: Conclusion and Future work.

1.3   Contributions

- Design, development, and preliminary evaluation of a soft-inflatable actuators of O and I cross-section and their comparison.

- Application of the inflatable actuators of I cross-section in a soft exosuit to assist knee swing during walking.

- Stiffness control of the soft inflatable exosuit with evaluation on three healthy test participants.

- sEMG study of knee extensors and flexors to evaluate effects of the exosuit.

- Design of fabric-encased soft-inflatable actuators for increased force output and application in an exosuit with improved control scheme.

- Investigation of knee kinematics, GRFs and sEMG for exosuit utilizing fabric encased inflatable actuators for 7 healthy participants.

- Evaluation of knee kinematics, GRFs, spatio-temporal parameters, Overground walking performance, and five time sit-to-stand performance on 3 participants undergoing post-stroke therapy.

- Design of a low-volume inflatable actuator composite and a portable pneumatic source for an untethered version of the exosuit.

SOFT-INFLATABLE EXOSUIT

2.1 Biomechanics of Walking
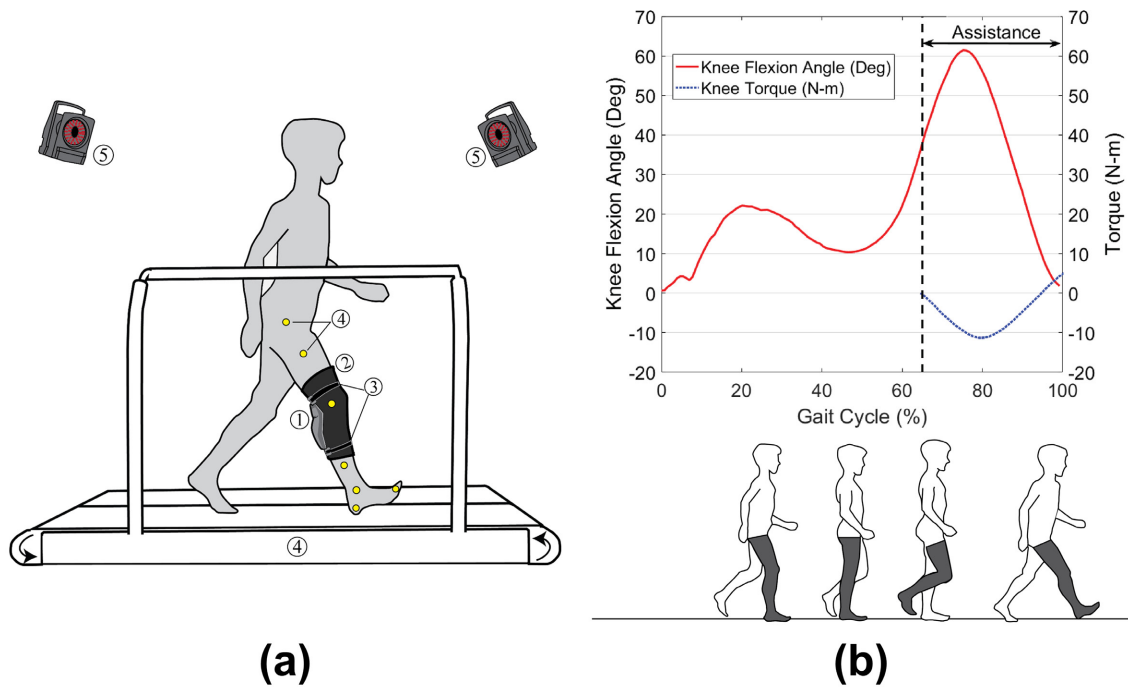
Figure 2.1 Profiles for Knee Angle and Knee Torque for Participant Walking at 1 m/s

To set the functional requirements for the soft knee exosuit and the soft-inflatable actuators, the behaviors of the knee joint and the muscles associated with the extension and flexion of the knee were investigated in existing literature. Additionally, an experimental study of the knee angles and torque generated during walking, was performed on an instrumented treadmill (side-by-side belt instrumented treadmill, Bertec Inc., Columbus, OH.) with ground reaction force recording capabilities. A motion capture system (T40s, VICON Inc., Los Angeles, CA.) with ten high-speed

infrared cameras was also utilized to create a complete kinematic model of the lower body. Passive reflective markers were placed on the ankle, hip and knee joints along with a set of markers on the thigh, shin, foot and toe of a healthy test participant as illustrated in Fig. 2.1(a).

The knee joint angles during the gait cycle and torques during the swing phase of walking were computed using inverse kinematics and dynamics following the methods described in [53]. From the computed knee angles and the ground-reaction forces obtained from the treadmill, the stance and swing phases of the gait cycle were established. The swing phase of walking was identified as ideal for providing knee joint extension assistance by aiding the quadriceps to complete the swing, as shown in Fig. 2.1(b).

Also, it should be noted that the knee joint in itself does not produce the torque, as in the case of motor driven exoskeletons [23]. The forces generated in the joint are due to the action of the muscles contracting and relaxing, during motion. In a walking cycle, the peak torque generated during the swing phase of the leg was determined to be $22N \cdot m$ at a walking speed of 3m/s, and was also verified in other studies [53]. It should be noted that the exosuit is required to aid the user during rehabilitation instead of completely assisting the knee joint. Therefore, having rehabilitation of the quadriceps and the limitations of soft robotics in mind, a partial assistance of 20% ($4.4N \cdot m$) was set as the required torque to be provided to the knee joint during the swing phase.

2.2   Design of Soft-Inflatable Actuators

2.2.1   Inspiration and Design

To design the inflatable actuators to be utilized in the soft-inflatable exosuit, inspiration was drawn from classical beam theory. According to the Euler-Bernoulli beam deflection theory [54]:

$$\frac{d^2}{dx^2}(EI\frac{d^2w}{dx^2}) = q \qquad (2.1)$$

Here, the buckling force the beam q is directly proportional to the second moment of inertia I and the elastic modulus of the beam E. Also, the deflection in the beam w is perpendicular to the axis of the beam at a position x. For a constant deflection, the bending force required would be directly proportional to the moment of inertia, I for a fixed material.
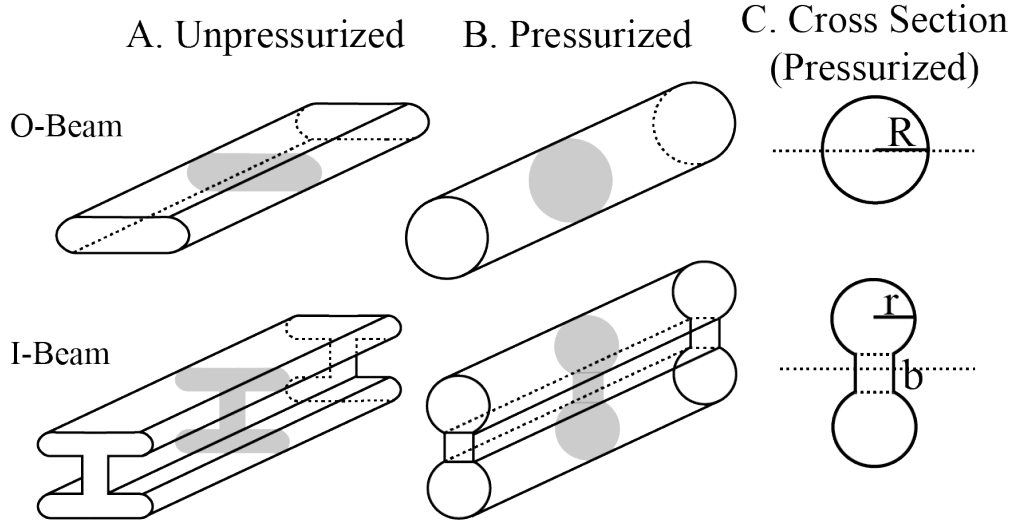
Figure 2.2 Layout of Inflatable Actuators of O and I Cross-section. (A) Unpressurized State of Both Actuators. (B) Pressurized State. (C) Sectional View of Actuators When Inflated.

As per beam theory, the moment of inertia of an I cross-section is higher than that of an O cross-section for the same cross-sectional area. Therefore, in this work, two different actuator types with I and O cross-sections are explored. The two actuators are compared for their ability to resist buckling at the same internal pressure. It is noted that the actuators when not inflated do not have the capability to resist bucking and the stiffness of an actuator is dependent on the internal pressure. The cross-section of the actuator changes upon pressurization as can be seen in Fig. 2.2B. The O cross-section actuator is assumed to take up a circular cross-secton while the I cross-section is approximated to be two circles and a square as shown in Fig. 2.2C.

Actuators of I and O cross-section were designed for the same cross-sectional area and the length for comparison of the bending force. The relation between the cross-sectional area of the I and the O cross-section is as shown in Equation 2.2 where R is the radius of O cross-section, r and b are the radius of the circle and side of square of the I cross-section when inflated.

$$\pi R^2 = 2\pi r^2 + b^2 \tag{2.2}$$

$$R = \sqrt{\frac{2\pi r^2 + b^2}{\pi}} \tag{2.3}$$

Upon rearrangement of Equation 2.2, R can be expressed in terms of r and b as shown in Equation 2.3. This allows for representation of the radius of the actuator of O cross-section in terms of the parameters of the actuator of I cross-section. The moment of inertias, for both the cross-sections were computed using the parallel axis theorem and are as follows:

$$Io = \frac{\pi}{4}R^4 = \frac{\pi}{4}[\frac{2\pi r^2 + b^2}{\pi}]^2 \tag{2.4}$$

$$Ii = \frac{5\pi}{2}r^4 + 2\pi br^3 + \frac{\pi}{2}b^2r^2 + \frac{b^4}{12} \tag{2.5}$$

14
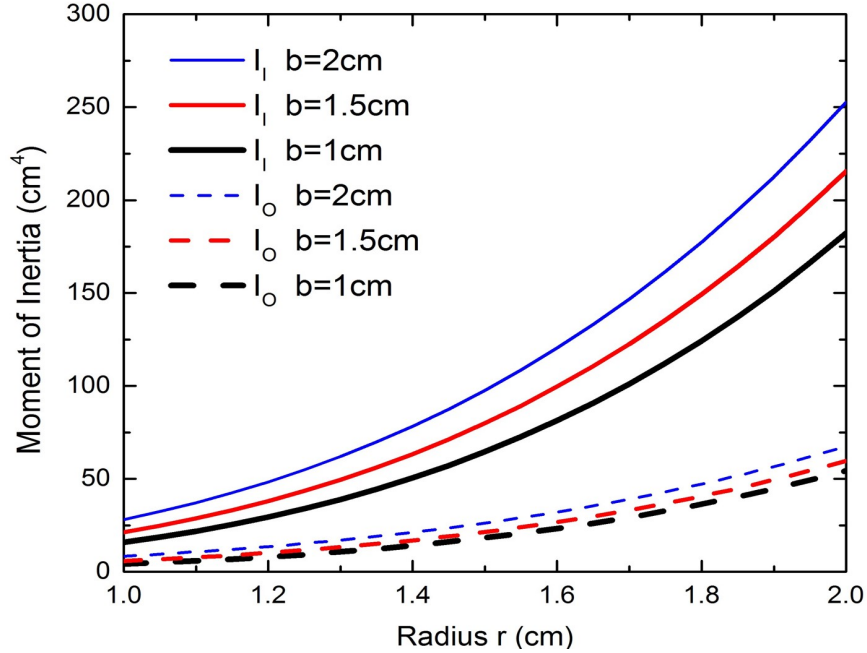
Figure 2.3 Variation of Moments of Inertia for the Actuators of O and I Cross-section with the Change in Values of r, b, and r Following the Relation 2.3.

The moment of inertias of the actuators of O and I cross-section are represented using Io and Ii respectively. Solving Equations 2.2-2.5 shows that the moment of inertia of the I cross-section is always greater than the O cross-section of the same sectional area. A graphical illustration of the possible solutions is as provided in Fig. 2.3.

2.2.2 Fabrication of Soft-Inflatable Actuators

The actuators are fabricated by heat sealing pieces of thermoplastic polyurethane (TPU) together. The actuator of O cross-section is fabricated using two layers sealed on all four sides. The actuator of I cross-section is fabricated in a similar manner by sealing multiple layers of TPU to create three chambers with varying dimensions to create the I shaped cross-section. Pneumatic fittings are incorporated 2.5cm from the seal to supply pressurized air. Figure 2.4 shows the prototypes as well as fabrication
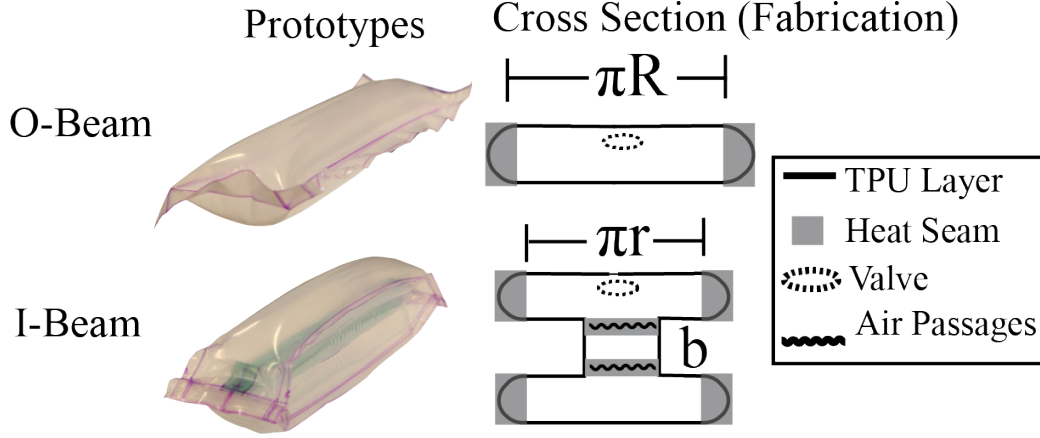
Figure 2.4 Inflatable Actuators of O and I Cross-section. (Left): Prototypes (Right): Fabrication Method for Actuators.

method of the actuators of O and I cross-section.

Based on the area available to incorporate the soft-inflatable actuators and the dimension of the femur and the tibia, the parameters for the actuator were selected. The parametric dimensions chosen for the fabrication of the actuators of O and I cross-section are $R=1.94cm$, $r=1.27cm$, $b=1.27cm$, and $l=25.4cm$ with $I_o=2.94cm^4$ and $I_i=36.99cm^4$. Two different materials – DT2001 with thickness of 0.1524 mm (American Polyfilm Inc., Branford, CT.) and Stretchlon 200 with thickness of 0.0381 mm (Fibre Glast Dev. Corps, Brookville, OH.)are explored for fabricating the actuators. It should be noted that different values of R, r and b can be utilized for the fabrication of the actuator of I cross-section given that Equation 2.3 is satisfied.

2.2.3   Characterization

Owing to the nature of the soft actuators, assistance during extension motion is generated. Keeping in mind that the goal of this work is to design an exosuit for the knee joint, a test setup was designed to evaluate the capabilities of the actuators to provide extension torque. It is hypothesized that if the soft-inflatable actuators

16
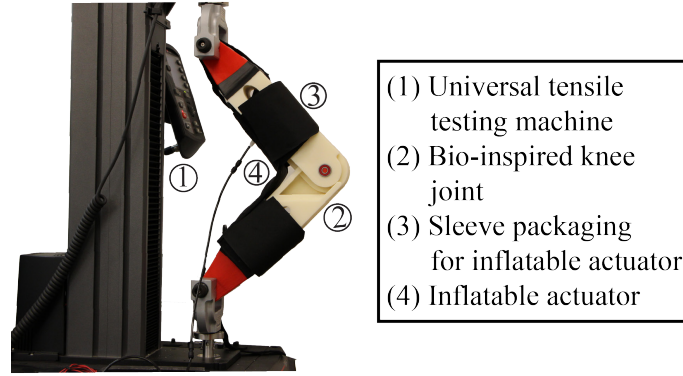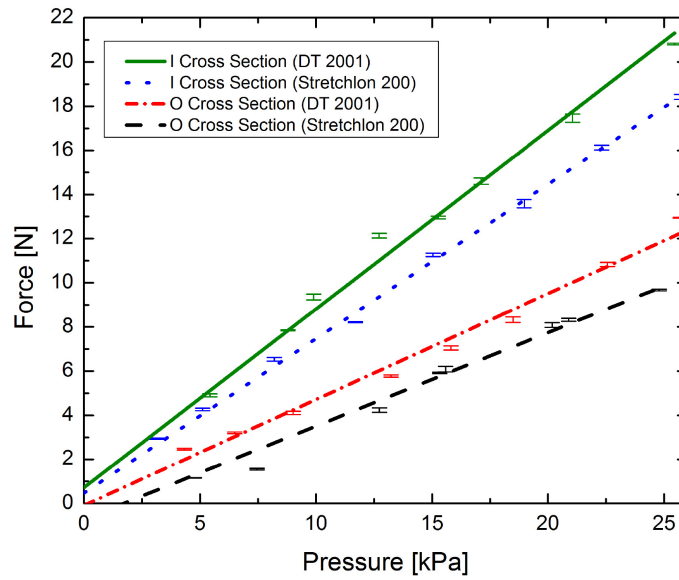
Figure 2.5 (A) Test Setup for the Characterization of the Soft-inflatable Actuator. (B) Force Profile for Increasing Pressure of I and O Cross-sections Utilizing Two Materials. Inflatable Actuator of I Cross-section Produces Higher Force Output as Compared to O Cross-section.

are placed in the knee pit and a pressure is applied, an assistive force to extend the knee joint can be generated hence aiding in the extension of the leg during the swing phase.

To mimic the knee joint in testing, a bio-inspired joint was created using acrylonitrile butadiene styrene (ABS) plastic using additive manufacturing (Fortus 450mc,

17

Stratasys, Eden Prairie, MN). The joint is designed in two pieces to replicate the femur and the tibia of the human body with a range of motion of 135°. For friction-less rotation, rotary ball bearings were incorporated at the center of rotation of the joint.

To mount the soft-inflatable actuators in varying configurations for more comprehensive testing, mounting points on the knee joints are signed. A fabric sleeve to attach the soft actuators to the knee joint is also fabricated to ensure that the actuator is equally spaced on the knee joint.

The force generated by the soft-inflatable actuators is measured using a universal testing machine(UTM) (Instron 5944, Instron Corp., High Wycombe, United Kingdom). The knee joint is mounted on the UTM with a fixed flexion angle of 60° as shown in Fig. 2.5 and the force is measured using a load cell while the actuators are pressurized. An angle of 60° is chosen akin to the maximum knee flexion angle during walking. The actuators are pressurized in intervals of 3.45 kPa and repeated three times for repeatability.

The actuators with O and I cross-section of the two different materials were tested. As seen from Fig. 2.5, the actuators with an I cross-section have a higher force output as compared to that with an O cross-section. Also, the DT2001 material shows a higher force output as well as higher durability under repeated loading and unloading when compared to the Stretchlon 200. Hence, inflatable actuators with an I cross-section and DT2001 material are utilized in the soft exosuit.

With the normal force generated by the actuator measured using the load cell attached to the UTM, the torque generated about the center of the knee joint is calculated. The force component perpendicular to the femur and tibia of the knee joint is calculated and the torque is calculated using the moment arm of the force. A single actuator is found to be capable of generating a torque of 2.2 $N \cdot m$ at 27.57 kPa. Therefore, two actuators of I cross-section are utilized in the soft exosuit.

2.3 Design of the Soft-Inflatable Exosuit

The soft exosuit consists of a fabric garment which is fashioned using a stretchable fabric (neoprene) to conform around the knee joint of the user. An inelastic fabric pocket to house the two inflatable actuators is sewn onto the fabric sleeve such that it aligns with the kneepit. The fabric pockets allow for the replacement of inflatable actuators in case of failure. Hook and loop straps are also sewn onto the fabric sleeve to firmly attach the exosuit to the user's leg. The straps allow for proper distribution of forces applied by the actuators to the user's leg while also preventing slippage. In addition to the straps, the inside of the fabric sleeve is lined with anti-slip material.

Figure 2.6 Design of the Soft-inflatable Exosuit. Inflatable Actuators Are Encased in a Fabric Sleeve with the On-board Electronics in a Separate Pouch. FSR Based Insole Sensor Are Placed in the Shoes.

To determine the walking pattern of the user, the soft exosuit system is equipped

with an insole sensor to sense the ground contact. The insole consists of two force-sensitive resistors (FSRs) enveloped in silicone (Ecoflex 30, Smooth-On Inc., Macungie, PA). The FSRs are placed at the heel and the ball of the feet to distinguish heel strike and toe-off. A fabric pocket is sewn on the fabric sleeve to house the micro-controller as well as the pressure sensor via a custom electronic board to allow for the use of multiple sensors. In total, the soft exosuit weighs 160g with on board electronic components.

The system consists of two 3 port-2 way electro-pneumatic solenoid valve (MHE3-MS1H valves, Festo, Hauppauge, NY), a pressure sensor (ASDXAVX100PGAA5, Honeywell International Inc., Morris Plains, NJ) to monitor actuator pressure, a pneumatic air supply and a vacuum pump. The solenoid valves are connected in a series configuration to facilitate inflation, deflation, and pressure holding capabilities. The addition of a vacuum pump allows for fast deflation of the inflatable actuators.

The primary goal of the exosuit is to provide user assistance during the knee extension part of the swing phase (mid-swing to terminal swing). The assistance would be maintained until the end of the gait cycle when the heel makes contact with the ground. Therefore, to provide appropriate assistance to the user, a binary controller is used in order to actuate the solenoid valves to inflate the exosuit, hence aiding in the knee extension if toe-off is detected. When heel-strike is detected, the actuators are deflated to allow knee flexion during pre-swing.

2.4 Preliminary evaluation of the Soft-Inflatable exosuit

To test the soft-inflatable exosuit on a test participant, the muscle activity of the quadriceps was studied. Surface electromyographic (sEMG) sensors were placed on the quadriceps (Vastus Medialis, Rectus Femoris, and Vastus Lateralis) of the user. The skin in contact with the sEMG sensors is cleaned prior to sensor placement to
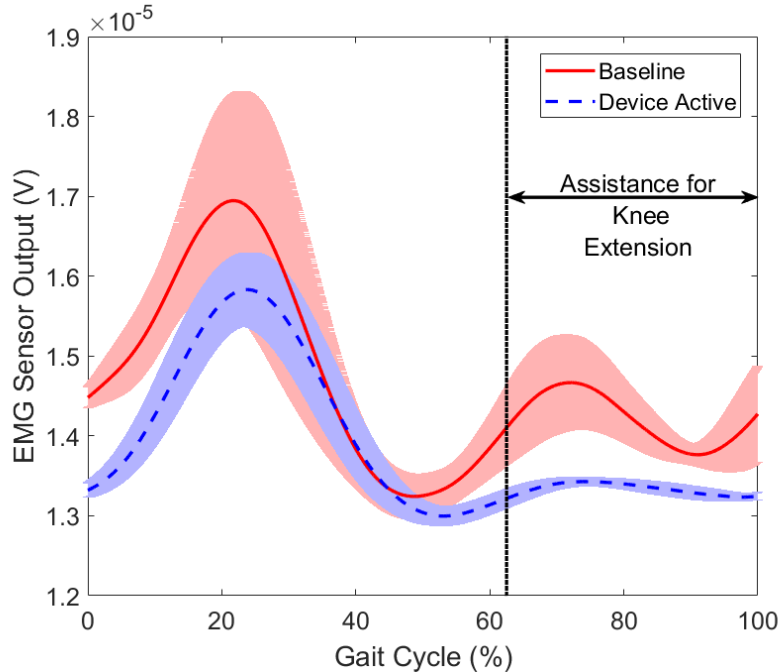
Figure 2.7 Muscle Activity of the Rectus Femoris Group for Participant Walking at a Speed Of 0.5 m/s Without Exosuit(Baseline) and with Exosuit(Device Active).

ensure clean quality of sEMG signals. The user is allowed to walk on an instrumented treadmill at speed of 0.5 m/s for 3 minutes with a 5 minute rest in between trials to eliminate effects caused due to fatigue. Safety precautions such as emergency stops are also incorporated to ensure safety of the test participant.

The sEMG signals are collected for a total of 6 trials with 3 trials without (baseline) and 3 trials with the exosuit active (device active). The collected data is processed using a fourth order Butterworth filter and averaged over five gait cycles. The compared for the baseline and device active conditions are compared for the Rectus Femoris muscle group as depicted in Fig. 2.7. A reduction of 7% is observed in the rectus femoris muscle group when the exosuit is active. A small reduction in the Vastus Medialis and Vastus Lateralis is also observed for all the collected sets of data.

Reduced muscle activity during the stance phase is also observed in the Device

Active tests. This can be attributed to the latency in deflation of the inflatable actuators which provides additional support to the quadriceps during the stance phase. A drift in the FSR based insole is also observed which could lead to faulty gait detection, leading to inappropriate assistance. However, due to the short span of experiments performed, the drift did not affect the tests performed. These issues will be addressed in Chapter 3.

Chapter 3

A CONTROL METHOD FOR THE SOFT INFLATABLE EXOSUIT

The initial version of the soft inflatable exosuit utilized a simple on-off control scheme which is prone to providing inaccurate assistance during walking. In order to accurate assistance using a wearable robot, the biological torques generated by the user as well as torques generated by the inflatable actuators need to be modeled. Furthermore, sensing modalities for the exosuit to provide feedback to the control system are critical.

Building upon the drawbacks of the first version of the soft inflatable exosuit which provided preliminary evidence of a wearable device that provided knee extension assistance during walking, this chapter presents the integration of the soft inflatable exosuit system with knee angle and advanced gait sensing methodologies. A control method utilizing knee quasi-stiffness models as well a data-driven actuator stiffness model is presented. Furthermore, testing and evaluation of the exosuit system and controller is performed using gait studies. The key contributions of this chapter are as follows-

- Design improvements to the soft inflatable actuators utilizing larger ports for faster actuation of the exosuit.

- Integration of the soft exosuit with inertial measurement units and smart shoe insole sensors for accurate knee angle measurement and gait phase sensing.

- A model for the quasi-stiffness of the human knee joint.

- A data-driven stiffness model for the inflatable actuators with an I cross-section.

- A controller that utilizes the biological quasi-stiffness model and actuator stiffness model for provide knee extension assistance during the swing phase.

- Evaluation of the exosuit and control scheme with three healthy test participants.

3.1   System Design

Figure 3.1 (a) Inflatable Actuators of I Cross-section. (b) Off-board Control Unit. (c) Imus on the Exosuit (d) *Smart Shoe* Insole Sensors.

3.1.1   Soft Inflatable Exosuit

Several design improvements were made to the soft exosuit following the preliminary testing. The modifications such as larger fluidic lines and improving the air flow profile of the actuator for expedited air flow are inspired by the results obtained through the first version of the exosuit. A pressure sensor is also attached directly to the actuator to eliminate the fluctuations caused by the rapid inflation and deflation

of the actuators for accurate pressure feedback.

3.1.2   Off-board Control Unit

In addition to the design modifications to the exosuit, an off-board control unit is designed to house the electro-pneumatic system such as the high speed solenoid valves(MHE3-MS1H valves, Festo, Hauppauge, NY) and integrated pressure sensors (ASDXAVX100PGAA5, Honeywell International Inc., Morris Plains, NJ). The control unit is equipped with a micro-controller (Raspberry Pi 3, Raspberry Pi Foundation, United Kingdom) to control the valves based on the sensory inputs. An air compressor is utilized to supply air pressure to the actuator and a vacuum pump is used to aid in deflation of the actuators. An emergency stop is also added to the system in accordance to an institutional review board (IRB) in the event of system malfunction to protect the user. Additionally, quick connect pneumatic fittings are utilized for fast setup and ease of transport of the system.

3.1.3   Knee Angle and Gait Measuring System

To identify the gait events and calculate the knee angle during walking, *smart shoe* insole sensors and inertial measurement units (IMUs) are added to the system. The *smart shoe* insole sensors consist of 4 sets of coiled silicone tubing attached to the sole of a shoe at the heel, toe, and the first and metatarsophalangeal joint. Each coil is a closed system attached to a pressure sensor which reads the change in pressure upon compression. This change in pressure is calibrated to standardized loads to determine the ground reaction forces (GRFs) during walking. The pressure readings are broadcasted through an ad-hoc network to the micro-controller and the gait events are identified using fuzzy logic [55]. Combining output from the multiple sensing points can be utilized to determine distinct gait events such as heel strike,
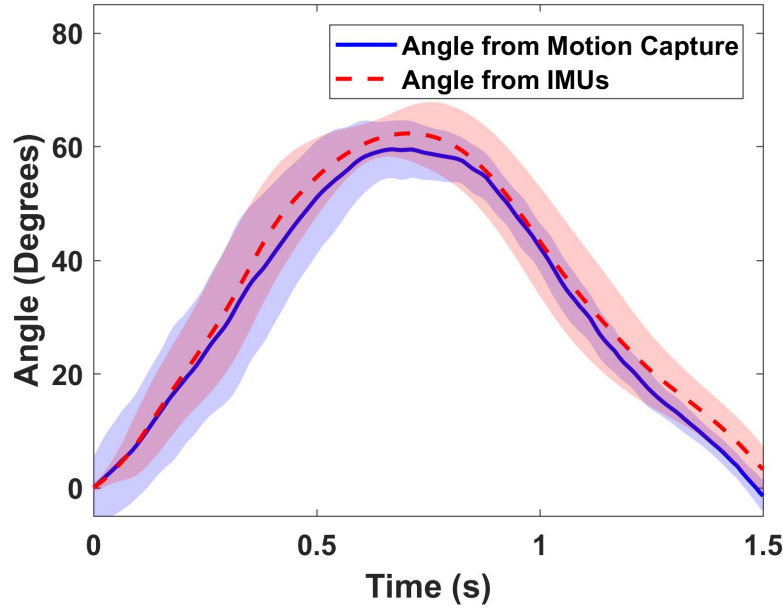
Figure 3.2 Comparison of Knee Joint Angle Measured Using Inertial Measurement Units and Motion Capture System with Standard Deviation. An RMSE Value of 0.19°, and Error of 0.32% Is Observed.

mid-stance, and toe off.

The IMUs used to measure the knee angle has 9 degrees of freedom (DOFs) with a 3DOF gyroscope, 3DOF accelerometer, and a 3DOF magentometer. The accelerometer and the gyroscope are utilized to estimate the knee angle and a gradient descent filter is utilized to ([56]) to the raw IMU data to eliminate high frequency noise and sensor drift. To estimate the knee angle during walking, two IMUs-one on the femur and one on the tibia are used as shown in Fig. 3.1(c). The IMUs are placed parallel to the limbs and parallel to the frontal plane to eliminate the effects of yaw and pitch. The knee angle is calculated by comparing the roll angles of the IMUs and the data is broadcasted to the microcontroller through the aforementioned wireless ad-hoc network.

The accuracy of the knee angle measurement system was evaluated by mounting the IMUs on the femur and tibia of the artificial knee joint (Discussed in Chapter 2). Passive reflective motion capture markers are placed on the rotational joint, femur, and tibia of the analog leg. The data from the IMUs and the motion capture system are recorded as the leg joint is moved and the angles obtained from both the systems are compared with the motion capture as the reference. A root means square error of 0.19° is obtained when the angles obtained from the IMUs and the motion capture system as observed from Fig. 3.2. This is an acceptable accuracy when compared to traditional angle measurement systems such as encoders [57]. The use of IMUs offers free motion with an acceptable measurement accuracy with a lightweight setup where the use of rigid mechanisms is not viable.

3.2   Control System Design

3.2.1   Modeling of Knee Stiffness

To model the stiffness of a healthy human knee joint during walking, the lower-body kinematics and the GRFs are collected using the motion capture system and the instrumented treadmill during walking. The knee torque is calculated using the plug-in gait dynamic model using inverse dynamic relations. As seen in Fig. 3.3, the gait cycle can be distinctly divided into the swing and the stance phase. The knee stiffness is defined as the slope of the profile obtained when the knee moment is plotted against the knee angle. To generate a mathematical model for knee stiffness, the system is assumed to be a spring-damper system and the relation between the knee moment and the knee angle is defined in [58].

$$T(s) = (Is^2 + Bs + K)\theta(s) \qquad\qquad (3.1)$$

27
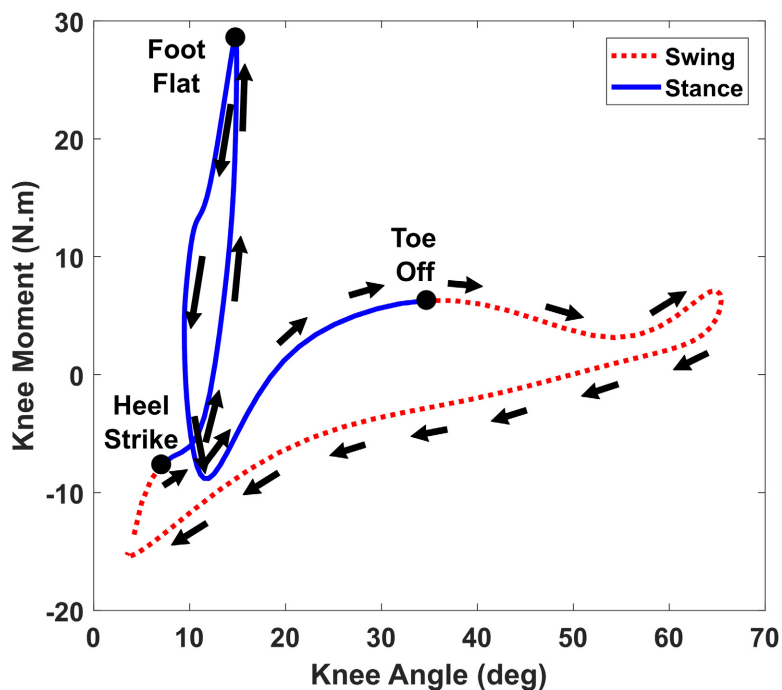
Figure 3.3 Knee Angle Versus Knee Moment for a Healthy Participant. The Knee Quasi-Stiffness at any Given Instant is Determined by Calculating the Slope of the Curve.

where, T is the torque, θ is the angle, I is the inertia, B is the viscosity and K is the stiffness of knee joint.

Since the soft exosuit is intended to be used in physical rehabilitation at slow walking speeds, the influence of the inertia and viscosity term are not significant and can be ignored. The averaged knee stiffness during the swing phase is calculated using the MATLAB System Identification toolbox and is determined to be 1.07 N·m/deg at a walking speed of 0.5m/s.

3.2.2 Data-driven Modeling of Inflatable Actuators

To model the stiffness of the soft inflatable actuator at varying flexion angle, test apparatus as described in Chapter 2 is used. The force generated by the actuator at varying pressure is measured using the load cell attached to the UTM under quasi-

28
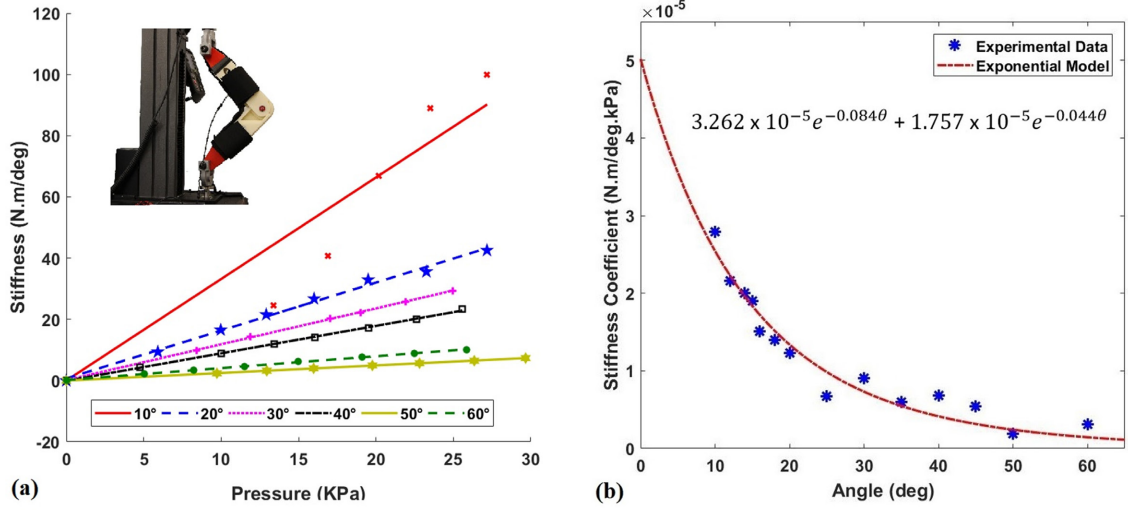
Figure 3.4 (a) Characterization of Actuator Stiffness at Angles Varied by 10° for Increasing Pressure with Test Setup in Inset. (b) Relation Between Flexion Angle $\theta(deg)$ and Coefficient of Stiffness $K(\theta)$ ($N \cdot m/deg.kPa$).

static conditions. The stiffness of the actuator is calculated for 0° to 60°. The flexion angle of the artificial leg joint was varied in 10° intervals and pressurized up to 27.58 kPa in intervals of 3.45 kPa. As seen from Fig. 3.4, a linear relation between pressure and stiffness is obtained at all angles. Therefore, to simplify the stiffness model for the inflatable actuators, a linear relation between pressure and stiffness is assumed with a stiffness coefficient which is a function of the flexion angle as shown:

$$S = K(\theta) \cdot P \tag{3.2}$$

where, S is the actuator stiffness, θ is the bending angle, and $K(\theta)$ is the actuator stiffness coefficient as a function of the angle.

The generalized equation stiffness coefficient $K(\theta)$ is obtained by plotting the slopes of the stiffness versus their corresponding flexion angles, as seen fin Fig. 3.4(b). Non-linear least squares method is used to fit an exponential curve to the data and the generalized equation for the actuator stiffness coefficient as a function of flexion

29

angle θ is as shown in 3.4(b). Owing to the nature of the model, a large change in stiffness is observed at lower angles while a very small change is seen at high values of flexion angle.

3.2.3 Control System Overview

A control system is designed in order to manipulate the actuator stiffness during the swing phase using control inputs from the IMUs and the *smart shoes*. As observed in Fig. 3.5, the controller is subdivided into two layers. The actuator stiffness profile is generated by the first layer using the knee angle generated by the IMUs and the gait events provided by the *smart shoes* to provide 25% of assistance at all times during the swing phase. Therefore, a reference stiffness profile S_{ref} is generated using these inputs. The desired pressure P_d is calculated using the knee stiffness reference
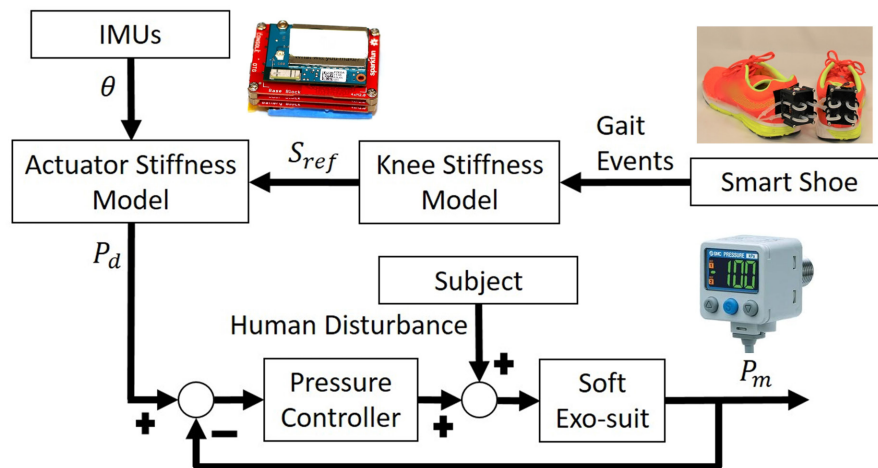
Figure 3.5 Two Layer Controller for the Soft Inflatable Exosuit. Gait Information from the *Smart Shoes* and Knee Angle from the IMUs is Utilized to Generate Desired Knee Stiffness. A Low Level Pressure Controller is Utilized to Track Desired Pressure Using Feedback from Pressure Sensor.
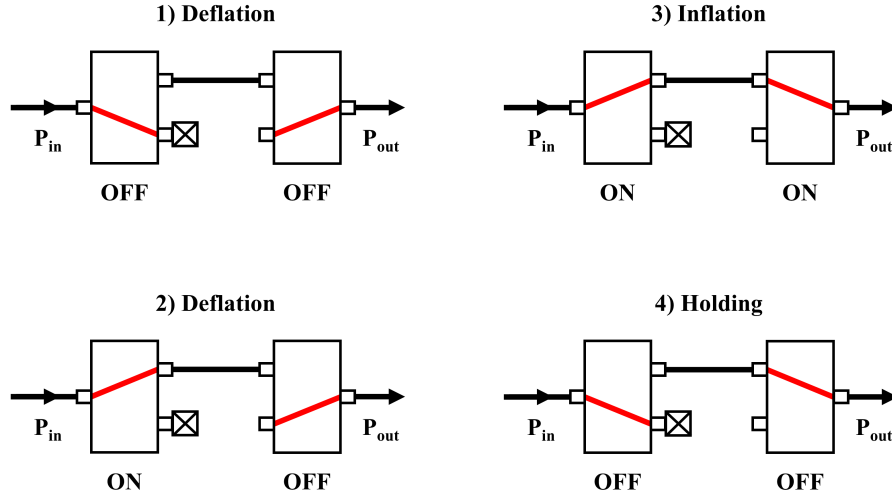
Figure 3.6 Series Configuration Using Two 3 Port - 2 Way Solenoid Valves. The Possible States Using the Two Valves are Demonstrated.

S_{ref} and the knee angle θ.

The desired pressure P_d is tracked using the second layer low-level controller which uses the pressure sensor feedback to manipulate the solenoid valves to control the inflation and deflation of the inflatable actuators. The closed loop low-level controller utilizes a combination of binary valves as seen below.

With the two 3 port - 2 way valves placed in a series combination, there are four possible combinations as shown in Fig. 3.6. Therefore, a total of three states using a combination of two binary valves are possible - Inflation, Deflation and Holding. Hence, to control the soft inflatable exosuit, the aforementioned states are utilized.

3.2.4   Pressure Tracking

The performance of the control system was tested through pressure tracking experiment. The high-level controller generates a desired pressure profile and the low-level controller is allowed to track the desired pressure profile. As seen from Fig. 3.7, the
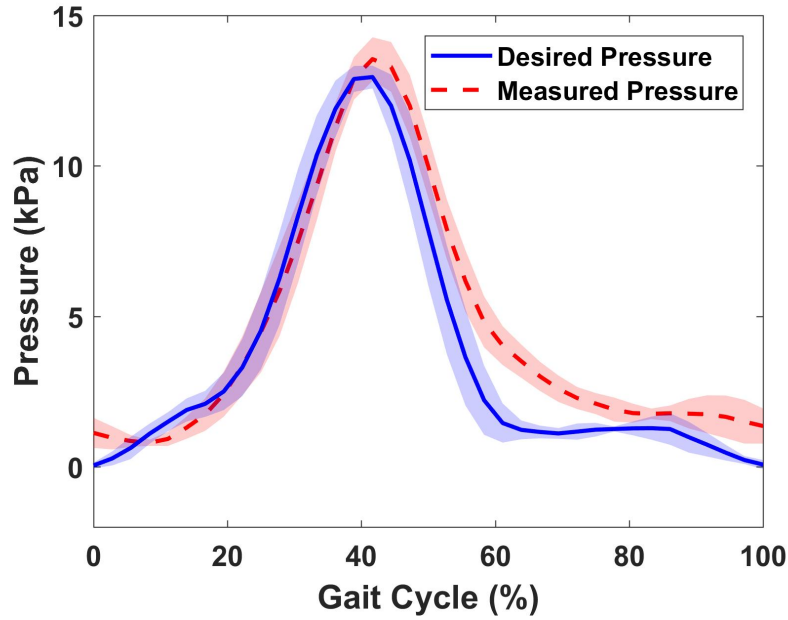
Figure 3.7 Pressure Tracking Performance of the Low Level Controller Averaged for Multiple Gait Cycles. An RMSE Value of 1.2 kPa and Error of 8.46% is Observed.

low-level controller is able to track the desired pressure with a small latency in the deflation at lower pressures. This is owing to the fact that the flow rate is directly proportional to the pressure gradient. The latency in deflation could also be a causality of the constant flow rate provided by the vacuum pump and the small size of ports leading to retardation of air flow.

Despite the observed overshoot at the maximum pressure, an Root Mean Square Error (RMSE) value of 1.27 kPa, shows fairly acceptable pressure tracking performance at lower walking speeds.

3.2.5 Exosuit Testing Protocol

To test the soft inflatable exosuit, three healthy test participants are recruited (anthropometric data shown in Rable 3.1). A written informed consent is obtained

No.	Gender	Age (years)	Weight (kg)	Height (m)
1	Male	25	65	1.72
2	Male	26	80	1.74
3	Male	25	79	1.65

Table 3.1 Anthropometric Data of the Three Participants Recruited for the Study.

from the participants, under an Arizona State University IRB approval(PHX-17-0145-70-21). The quadriceps and the hamstrings of the participants thoroughly cleaned using alcohol wipes. The appropriate placement for the sEMG sensors are identified using the guidelines provided by the Seniam protocol ([59]). The sensors are placed on the: Rectus Femoris (RF), Vastus Lateralis (VL), Vastus Medials (VF), Biceps Femoris (BF) and the Semitendinosus (ST) muscle groups as depicted in Fig. 3.8. The muscle activities at rest and at maximum voluntary contraction (MVC) are also collected for normalization.

The walking tests performed are similar to the test performed in Chapter 3. The participants are allowed to walk on the treadmill without the exosuit (Baseline) and with the exosuit (Device Active). For both the tests the soft inflatable exosuit is worn over the sEMG sensors to ensure that the same pressure is applied over the sEMG sensors for accurate signal comparison. A test without the exosuit not donned (Baseline condition) is not included in this study as the elastic sleeves used for the soft exosuit do not enhance performance in any way except proprioception ([60, 61]).

Following all safety requirements, as described in our IRB protocol, the non-impaired adult participants are instructed to walk on an instrumented treadmill with the sEMG sensors attached to the aforementioned muscle groups. The participants walk on the treadmill for three minutes at a slow speed of 0.5 m/s, followed by a
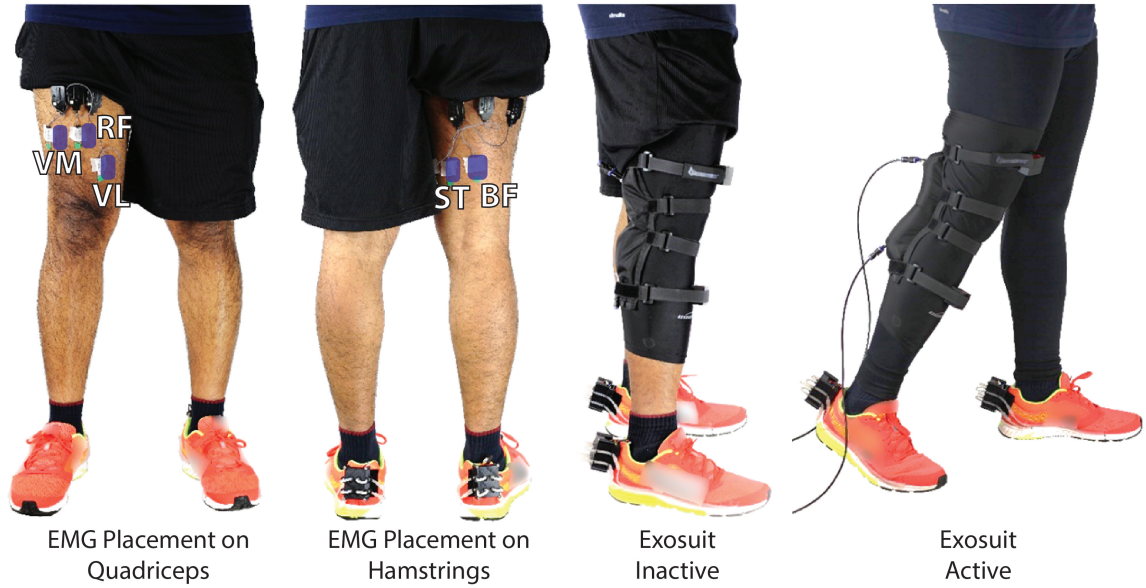
Figure 3.8 Test Protocol Setup with Positions of sEMG Sensors and Exosuit Inactive and Active Conditions.

rest period of five minutes between the baseline and active phases. Each of the test phases is performed three times to ensure accuracy of the collected muscle data (A total of six times for both baseline and device active).

3.2.6 Participant Testing

The collected sEMG signals from the walking tests are post-processed and filtered using a fourth-order Butterworth filter with a cut-off frequency of 15 Hz. The collected data is normalized to the base resting activity and the MVC muscle activity for individual muscle groups. Five gait cycles for each muscle group are averaged for both the baseline and device active conditions. The gait cycles used for averaging are picked from the same time window for accurate comparison. The data is selected from the middle one minute of the trial to ensure that the user is accustomed to the use of the exosuit while not adopting compensatory patters due to the assistance

34

provided by the exosuit.
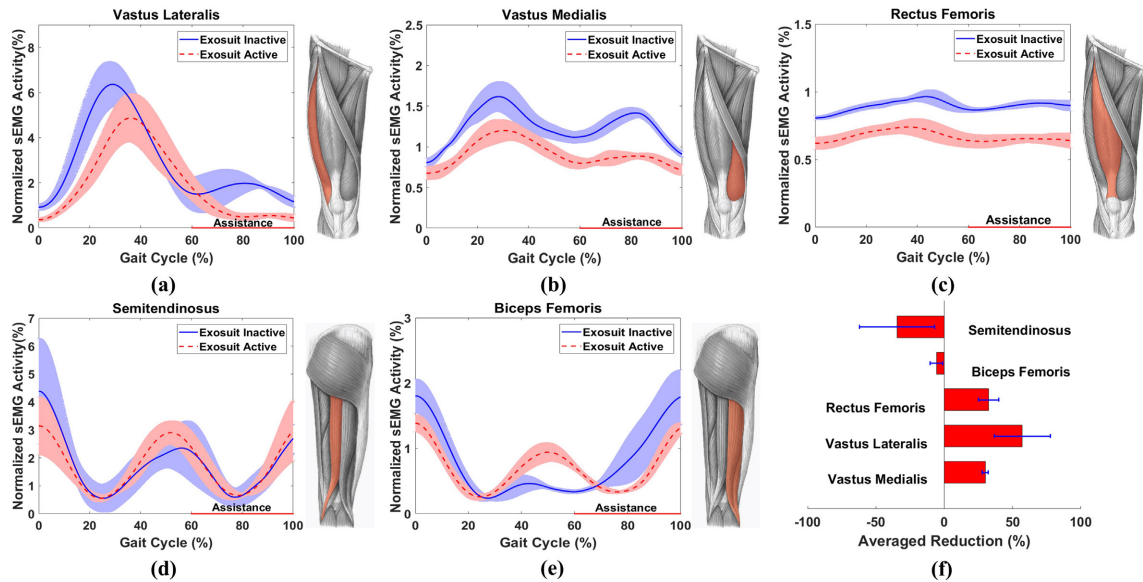
Figure 3.9 sEMG Activity of (a) VL, (b) VM, (c) ST, (d) RF and (e) BF Averaged for Five Gait Cycles. (f) Averaged Reduction for ST(n=3), BF (n=2), RF (n=2), VL(n=3), VM (n=3).

The muscle activities of the five groups and their corresponding reductions are provided in Fig. 3.9(a)-(e). An overall reduction of 57.16%, 30.06%, and 32.5% is observed in the muscle activity of the VL, VM, and RF, respectively. Therefore, the soft inflatable exosuit reduces muscle effort for the primary knee extensors [62].

An increase of 5.7% and 34.56% in the BF and ST respectively is also observed when the exosuit is active potentially due to the latency in actuator deflation. This latency also causes a decrease in the activity of the quadriceps during the stance phase providing knee support during heel stike and initial stance phase of the test participants. The increased hamstring activity could also be a result of early detection of swing phase.

The improvement of the low-level pressure (PWM) controller using pulse width modulation, addition of delays during inflation to actuate during mid-swing, improving the exhaust rate by adding larger ports and fluid lines, and testing of impaired participants to investigate biomechanics and the effectiveness of the exosuit, are addressed in Chapter 4.

Chapter 4

ASSISTING KNEE EXTENSION IN THE SWING PHASE AND INITIAL

STANCE USING THE SOFT INFLATABLE EXOSUIT

This chapter further evaluated the design of the soft inflatable exosuit by testing knee extension assistance during the swing phase and initial stance of walking. Several design modifications to the exosuit were made in order to improve torque output capabilities of the exosuit as well as inflation and deflation of the system. Further the controller of the exosuit was modified in order to account for the knee flexion during the swing phase of walking. The exosuit was evaluated with seven healthy participants examining the lowerbody kinematics, ground reaction forces, and sEMG activity of the knee extensors and flexors. The exosuit was applied to three participants undergoing post stroke physical therapy. The lowerbody kinematics, ground reaction forces, spatiotemporal parameters, compensatory gait patterns, and overground walking using a timed up and go test. The major contributions of this chapter are as follows -

- evaluations of knee extension assistance during the swing phase and initial stance with healthy participants (n=7) . Lower body kinematics, surface electromyographic (sEMG) activity of the knee extensors and flexors, and ground reaction forces (GRFs) in treadmill walking are analyzed.

- evaluations of the soft exosuit with participants undergoing post-stroke therapy (n=3). Knee kinematics, spatio-temporal parameters, GRFs, and compensatory gait patterns (circumduction and hip-hiking) are explored to demonstrate the immediate benefits to the users through knee extension assistance during tread-

37

mill walking. In addition, a timed up-and-go (TUG) test is performed to study potential improvement of overground walking speeds with the exosuit.

4.1 Significance of knee extension in Swing phase and Initial Stance

Stroke survivors often demonstrate reduced muscle control, strength, and spasticity in their lower body muscles such as the hamstrings, quadriceps, plantar and dorsi flexors. Due to the aforementioned issues and deficits, they adapt their walking pattern to locomote. Literature on stroke gait shows that reduced knee extension prior to heel strike is a common characteristic of hemiplegia [63].

Moore et. al. hypothesize that causes of the smaller knee extension are as follows-

- Reduced tension in knee extensors during early swing.

- Increased tension in the knee flexors.

- Reduced knee flexion during swing phase which leads to reduced knee extension prior to heel strike.

Therefore assisting knee extension in the swing phase of walking can aid in reducing the aforementioned kinematic deficit. Also, reducing the deficit in knee angle during initial contact or terminal swing can lead to improvement in limb advancement.

During the initial stance and loading response in stroke survivors, another commonly observed problem is knee buckling. Prior work has identified the cause of buckling as unstable knee flexion moment as well as weakened quadriceps [64]. Due to reduced control and strength in the quadriceps, the stance limb is not able to take the weight of the body and collapses. A common gait compensation utilized by the stroke survivors to overcome bucking is the use of knee hyperextension during walking. Therefore, assisting knee extension during initial stance could potentially aid in better gait quality in stroke survivors.
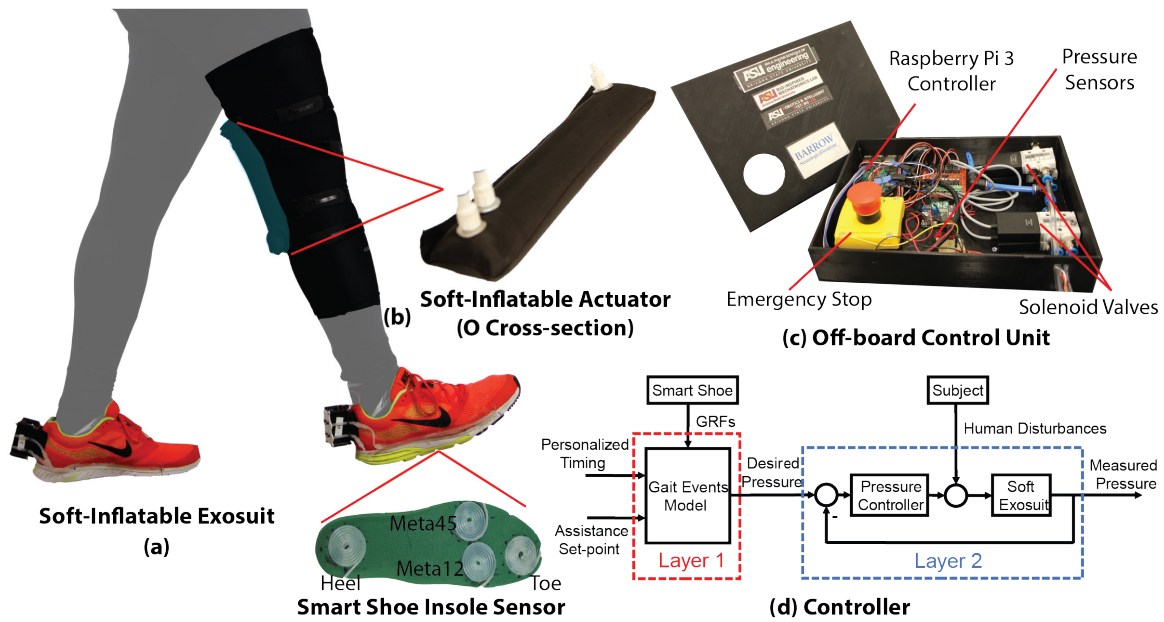
Figure 4.1 (a) The Soft Inflatable Actuator Applied to a Participant (b) Fabric Encased Inflatable Actuators with an O Cross-Section (c) Off-board Control Unit in accordance with the IRB. (d) Controller Design for the Soft Inflatable Exosuit.

4.2 Design of the Soft Exosuit

Similar to the previous versions of the soft inflatable exosuit, the device is designed using a neoprene interface which is worn by the user. The inflatable actuators are housed in a fabric pouch that is placed at the popliteal fossa or the knee pit. To ensure that the soft inflatable exosuit (4.1(a))could assist impaired participants to perform knee extension, certain design changes were made. The torque required to assist participants who suffered a stroke is higher due to the lack of muscle strength and the muscle spasticity. Therefore, inflatable actuators encased in fabric (Fig. 4.1(b)) were utilized. The advantage of using encased actuators is that due to the strength of the material, a higher pressure can be applied to the actuators which leads to a higher force output [65]. Therefore, as opposed to the previous designs, the exosuit is able to generate the maximum knee torque required during swing phase ($22N \cdot m$)

39

[53]. Also, to expedite the flow of air through the actuators, an additional port was added. A torque sensor is not included in this work in order to reduce the weight of the exosuit and allow the system to be highly compliant. It should be noted that the soft inflatable exosuit is intended to not impede the movement of the participant when the actuator is inactive.

An off-board control unit as shown in Fig. 1(c) is utilized to provide pressure input to the soft inflatable exosuit. An air compressor acts as the main pressure source and the air flow is controlled using solenoid valves (MHE3-MS1H valves, Festo, Hauppauge, NY). The control input for the solenoid valves is generated using a microcontroller (Raspberry Pi 3, Raspberry Pi Foundation, Cambridge, United Kingdom). The actuator pressure is monitored using a fluidic pressure sensor (ABP-MANN004PGAA5, Honeywell International Inc., Morris Plains, NJ). The inflation and deflation of the soft exosuit are triggered using gait phase information, provided by smart shoes. Additional information on the inflatable exosuit system as well as smart shoe insole sensors are detailed in Chapters 2 and 3.

4.3   Control

A two-layer control strategy is used to provide the personalized assistance during the swing phase, based on gait events during walking as depicted in Fig. 4.1(d). The first layer takes the GRF inputs from the smart shoe insole sensors [68], the maximum pressure for the actuators, and the inflation delay of the actuators. The stance and swing phases are discerned with the total GRF reading with greater than 10% of the bodyweight classified as the stance phase.

The maximum pressure and inflation delay inputs are used to calculate the desired pressures and timing of the inflation of the actuators which are selected individually for each participant to complete knee flexion during the pre-swing and swing phases
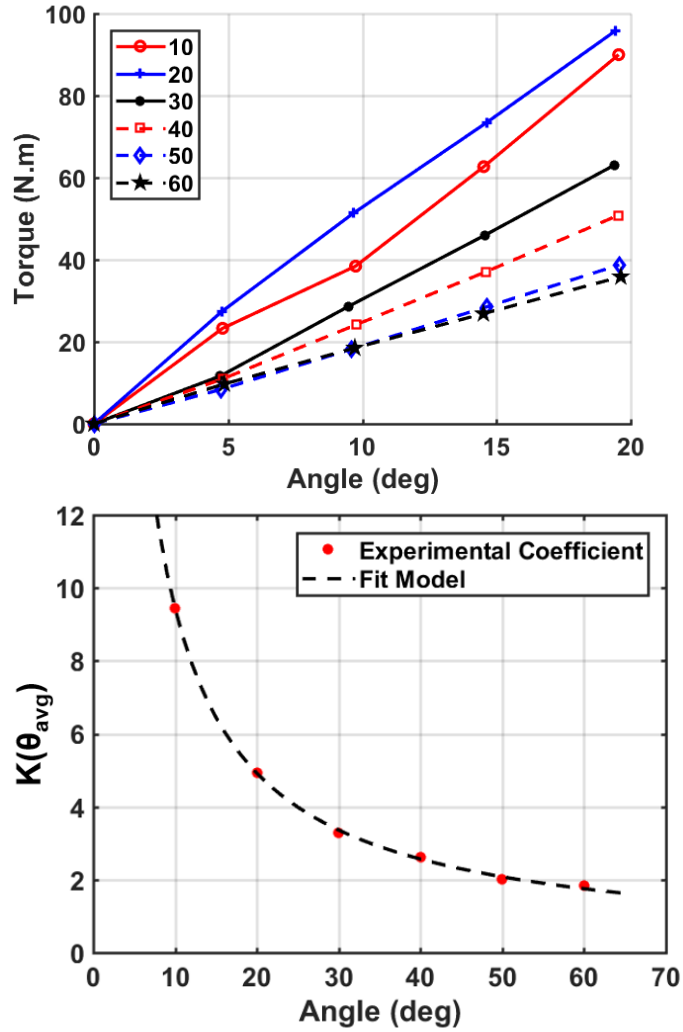
Figure 4.2 (Top) Actuator Characterization for Varying Angles. (Bottom) Curve Fitting Result for $\tau(\cdot)$.

and avoid rapid acceleration of the limb into extension. The desired inflation pressure and timing of inflation are selected individually for each participant to avoid rapid acceleration of the limb into extension and to allow for complete knee flexion during the pre-swing and swing phases.

The characterization of the inflatable actuators to provide extension assistance is as shown in Fig. 4.2. The actuators are mounted on an analog leg which is attached
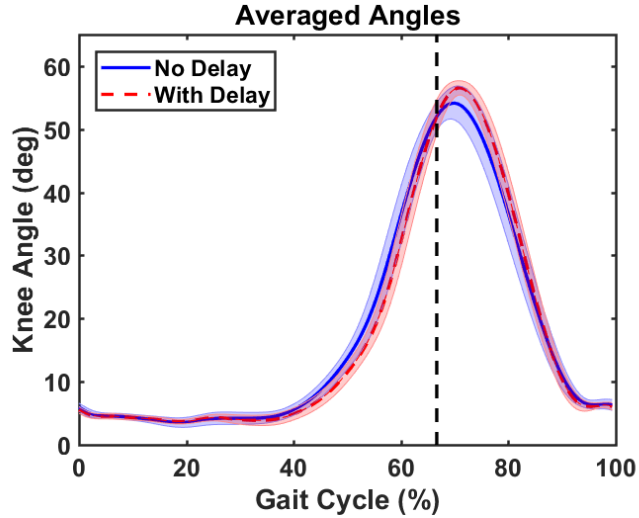
Figure 4.3 Knee Angles for One Participant With and Without Inflation Delay When Exosuit is Active and Assisting

to a universal testing machine. When inflated, the actuators apply a torque about the joint of the analog leg which is translated to a force which is read by the load cell. A model for the actuator torque is created using the data obtained. This model $K(\cdot)$ is used in the exosuit controller to provide assistance to the user.

The effect of adding a personalized timing delay for providing knee extension assistance is as shown in the Fig. 4.3. For this test, one participant was asked to walk on the instrumented treadmill set at a speed of 0.5 m/s when being assisted by the exosuit. The knee angles when assistance was provided with and without a time delay were measured. The peak flexion angle when the inflation delay is provided was observed to be higher when compared to when the assistance was provided with no delay. Therefore, with the inflation delay, the participant was allowed to complete knee flexion during early swing which was a drawback of the control methods used in Chapters 2 and 3.

The second layer consists of the soft exosuit and the electro-pneumatic system. A closed-loop feedback PID controller is used to track the desired pressure defined

by the first layer. Based on the error between the desired and measured pressures, the controller is designed to switch between the binary control (pure inflation or deflation mode) and pulse width modulation (PWM) control. If the absolute value of the pressure error is larger than a defined threshold, the valve configuration will remain in pure inflation mode or deflation mode for rapid reduction of the error. However, when the pressure error is small enough, the controller will switch to the PWM control. The PWM control unites five command cycles of the valves as one PWM duty cycle where maximum pressure error generates a PWM signal with five command cycles in inflation mode.

4.4   Healthy Participant Testing

To examine the effects of the soft exosuit on healthy participants and measure performance of the controller, a participant study is designed. The goal of this study was to see reduction in muscle effort for the quadriceps with minimal or no changes in the hamstrings. Also, the goal was to study how reduced knee angles at heel

Table 4.1 Anthropometric Data of the Healthy Study Population.

Participant	Gender	Age	Weight	Height	Assistance
H1	Female	23	65 kg	1.72 m	$10 N \cdot m$
H2	Male	23	82 kg	1.74 m	$10 N \cdot m$
H3	Male	22	69 kg	1.81 m	$10 N \cdot m$
H4	Female	23	78 kg	1.70 m	$10 N \cdot m$
H5	Male	25	70 kg	1.80 m	$10 N \cdot m$
H6	Male	22	71 kg	1.67 m	$10 N \cdot m$
H7	Male	26	77 kg	1.65 m	$10 N \cdot m$

strike could affect walking overall. Seven test participants were recruited for testing the soft exosuit. A written consent was obtained from all participants under an Arizona State University/Barrow Neurological Institute IRB (PHX-17-0145-70-21). The anthropometric data of the test participants is shown in Table 4.1.

Prior to testing, the recruited participants were prepared for the study by providing them a briefing of the test procedure performed. The regions on the skin in contact with the sensors and motion capture markers were thoroughly cleaned using alcohol wipes. The passive reflective motion capture markers and sEMG sensors were attached to the lower body of the participants using double sided tape. A total of 16 markers and 5 sEMG sensors were attached to the participant. The lower-body kinematics were extracted from the motion capture system using an in built model (VICON Plug-in Gait LowerBody). The sEMG sensors were placed on the quadriceps (VL, RF, and VM and the hamstrings(BF and ST).

The participants walk on an instrumented treadmill for 3 minutes at a speed of 0.3 m/s for both exosuit inactive and active. Also, a comparison for baseline walking with the exosuit garment being worn is performed to verify that the exosuit does not impede the user when inactive. The collected kinematics, sEMG, and GRFs are averaged for multiple gait cycles and compared for the inactive and active conditions. The ground reaction force data was utilized to segment each individual gait cycle. The EMG data was rectified and filtered using a moving weighted average filter. As compared to the fourth-order Butterworth filter utilized in Chapters 2 anad 3, the moving weighted average filter is not prone to shifts in data caused due to high filtering frequencies. The data was averaged for 300 samples and normalized to the maximum voluntary contraction (MVC). The inactive and active conditions were compared using the area under the sEMG curve.

For this study, the statistical analysis carried out using JMP PRO 13 software

(JMP, Cary, NC). A Student's t-test, Welch's t-test, or exact Wilcoxon rank test was used for identifying significance between the the different conditions. The type of test selected depending on the comparison being made. A power level of 0.8 was maintained while performing statistical analysis.

4.4.1   Lower-body Kinematics

The joint angles of the knee, hip, and ankle during walking are compared between the baseline, exosuit inactive and active conditions using the motion capture data. For comparison between baseline and inactive condition, no significant changes in knee angle were observed as shown in Fig. 4.4. The ankle angles for the baseline condition varied for all participants since exosuit did not impede the ankle joint during walking and the participants were allowed to self select their gait pattern.

The lower-body kinematics for two healthy participants (H_1 and H_2) as depicted
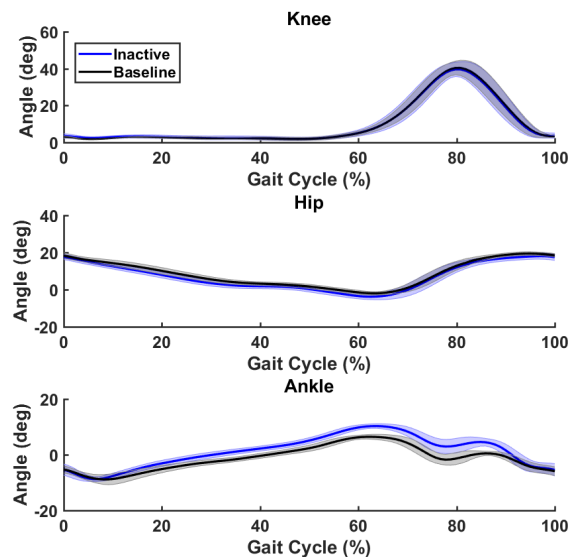
Figure 4.4 Comparison of Lower-Body Kinematics for the Baseline and Inactive Conditions. No Significant Changes in the Knee and Hip Angles were Observed.

45
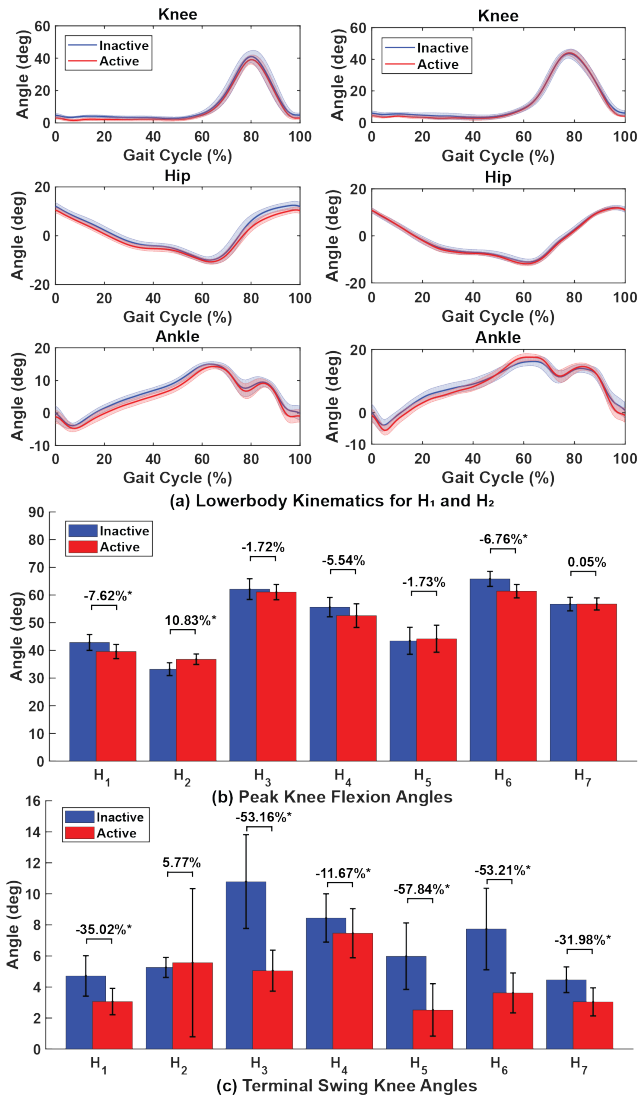
Figure 4.5 (a) Kinematics of Participants H_1 and H_2 During the Exosuit Active and Inactive Conditions (b) Maximum Knee Flexion Angle Compared for Exosuit Active and Inactive Conditions. Five Participants Demonstrated a Non-Significant Change in the Peak Knee Flexion Angle with H_1 and H_2 Showing a Decrease and Increase,R respectively. (c) Knee Angle at Terminal Swing for all Participants When the Exosuit is Inactive and Active. Reduced Knee Angle at Terminal Swing Was Observed for Six Participants.

in Fig. 4.5(a). A non-significant change at the peak knee flexion angle for four participants was observed as depicted in Fig. 4.5(b) whereas 2 participants presented a

46

decrease in peak flexion angle. Participant H_2 demonstrated an increased peak flexion angle during the exosuit inactive condition. Reduced knee angle at terminal knee swing is also observed for 6 of the 7 participants. This result was due to theassistance provided by the exosuit as seen Fig. 4.5(c). This indicates that the participants walk with a decreased knee angle at heel strike as well as early stance phase.

For further examining the kinematic effects of the modified knee angle during the gait cycle, the hip and ankle kinematics were examined. Some participants demonstrated a decreased hip angle during walking as seen in he case of H_1 while other participants did not demonstrate modified hip angles as seen with H_2. All participants demonstrated varying ankle angle patterns during walking which indicated a self selected gait adaptation.

Table 4.2 Muscle Responses for Each of the Investigated Muscle Group for All Healthy Participants for the Exosuit Inactive and Active Conditions. + and - Indicate an Increase and Decrease in Muscle Activity Respectively.

	ST	BF	VM	RF	VL
H_1	-8.46%*	+13.69%*	-9.28%*	-14.94%*	+0.68%
H_2	+10.37%*	-13.21%	+2.64%*	-8.99%*	-5.41%*
H_3	+1.15%	+10.37%	-3.83%*	-28.51%*	-0.8%
H_4	-0.83%	+24.79%*	-2.45%*	+0.34%	+5.56%*
H_5	$\times$	-23.73%*	-7.83%*	-4.70%*	-10.76%*
H_6	-8.05%	-18.69%*	-4.29%*	-2.07%	-1.23%
H_7	-3.03%	-19.15%*	-2.85%*	+0.79%*	-6.03%*
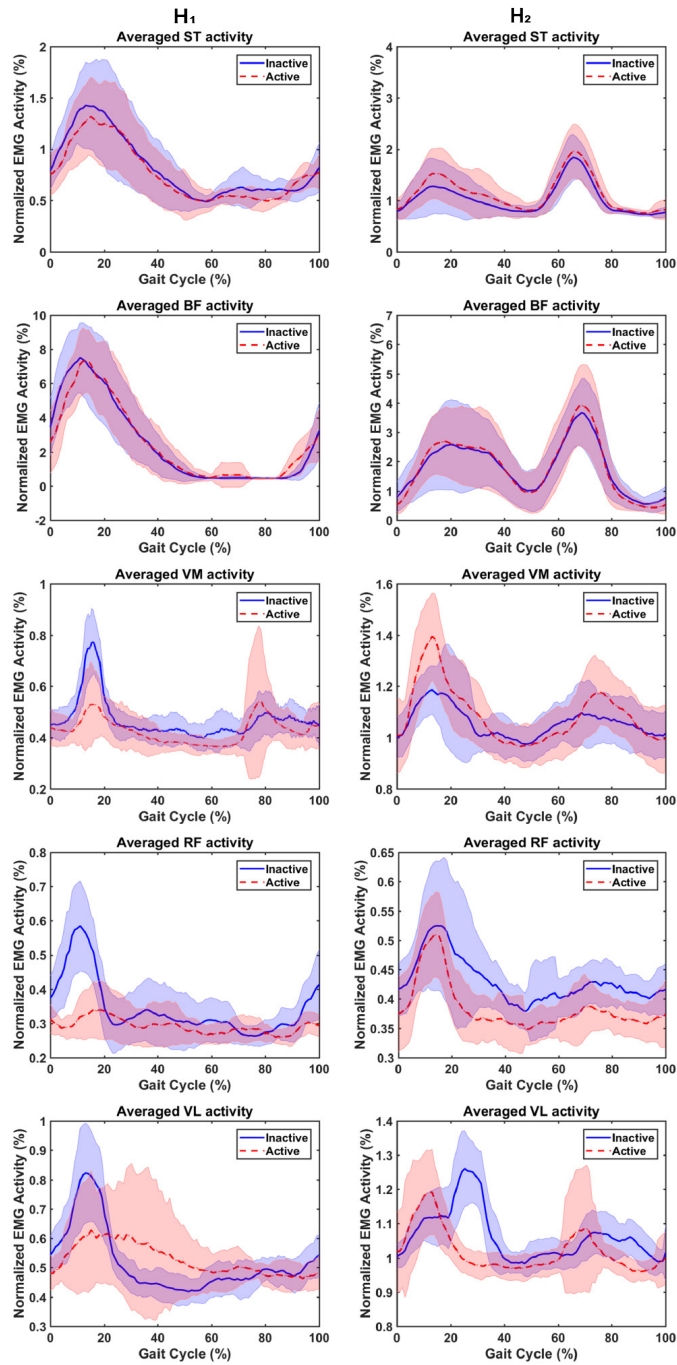
Figure 4.6 sEMG Activity of Participants H_1 and H_2 During the Exosuit Active and Inactive condition.

4.4.2 sEMG Comparisons

The sEMG data of the seven healthy participants collected during the inactive and active walking trials. The data collected from participants H_1 and H_2 are as depicted in Fig. 4.6. Both H_1 and H_2 demonstrated varying muscle responses during walking due to the adoption of different walking pattern. H_1 and H_2 demonstrated difference in hamstring activity with H_1 demonstrating an increase in BF activity during the stance phase and H_2 demonstrating an increase in ST activity during the pre-swing and swing phase of walking. Furthermore, in the stance phase both participants demonstrate varying VM activity. H_1 demonstrates a decrease and H_2 demonstrates an increase in VM activity during walking. It was observed that each participant adapted to the exosuit assistance in their own particular manner. This muscle activity adaptation is as detailed in 4.2. Further, the reduction in muscle activity during the stance phase was an added effect of the assistance provided during initial contact of the gait cycle. Overall, a reduction in the quadriceps for a majority of participants with no significant changes in the hamstrings was observed.

4.4.3 GRF Comparisons

The GRFs for H_1 and H_2 for the exosuit inactive and active conditions are presented in Fig. 4.7(a). Increased total GRF is seen for H_1 with non-significant changes for H_2. The heel force for all participants is also analyzed to investigate landing patterns when the exosuit is active. As seen in Fig. 4.7(b), increased peak heel GRF for four participants is observed whereas two participants show a significant decreases.
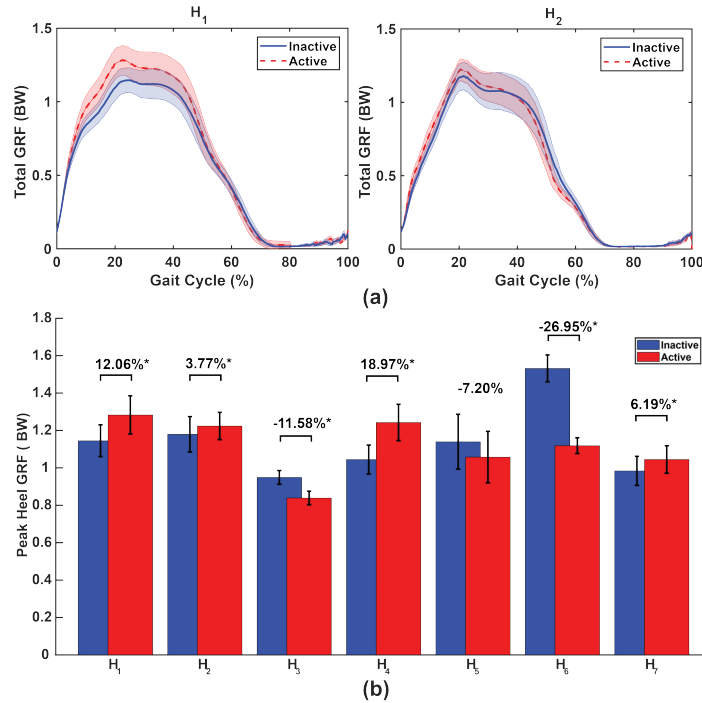
Figure 4.7 (a) Total GRFs for Two Healthy Participants (H_1 and H_2) When the Exosuit is Inactive and Active, Averaged Over Three Minutes. The Shaded Regions in the Figure Represent Standard Deviations of the Averaged GRFs. (b) Peak Heel GRFs for All Healthy Participants Compared Between Inactive and Active Conditions. An Increase in the Peak GRF Was Observed for Four Participants While Another Two Participants Demonstrated a Significant Decrease.

4.5 Impaired Participant Recruitment Criteria and Test Protocol

Participants with a primary diagnosis of stroke were recruited under the inclusion criteria, which involved the ability to independently walk overground and perform sit-to-stand transfers without the assistance of any aids such as canes and walkers. Participants having a modified Ashworth spasticity rating [69] of 3 or higher were excluded from this study due to the increased joint stiffness which would require large knee extension torques and could cause injuries. Participants under the age of 18 or weighing over 113kg were also excluded from this study. A manual muscle test (MMT)

50

was also performed to assess the strength of the participants. Participants with a MMT score of less than 3− were excluded from this study. A total of five participants were initially screened for the study and three were selected (anthropometric data listed in Table 4.3). It is noted that all three participants were affected on the right side. All the impaired participants held on the handrail when walking on the treadmill for safety guarantee.

In addition to the similar treadmill walking tests performed on healthy participants, a TUG test was performed for the impaired participants to assess overground walking. A mock-up test session was performed to gauge the ability of each participant. The lower-body kinematics for each participant were collected using the aforementioned motion capture system. The torque applied by the exosuit was decided based on the MMT scores and inputs from the therapists, as shown in Table 4.3.

The immediate effects of knee extension assistance were analyzed using step length, step time, leg circumduction and hip hiking during walking for the three impaired participants. All participants were allowed to walk at their most comfort-

Table 4.3 Anthropometric Data of the Hemi-paretic Study Population. The Manual Muscle Test (MMT) Rating for Knee Extension and Flexion. Ankle Foot Othotic (AFO) Users Were Allowed the Use of a Bandage to Hold Ankle Position.

	Gender	Age	Weight	Height	AFO	MMT	Assistance	Personalized Timings
P_1	Female	74	59.2 kg	1.65 m	No	4+ / 4+	$13\ N \cdot m$	0.3 s
P_2	Male	69	76.4 kg	1.72 m	Yes	3+ / 3-	$19\ N \cdot m$	0.3 s
P_3	Male	58	83.9 kg	1.85 m	Yes	4+ / 5	$13 N \cdot m$	0.2 s

able self-selected pace. Walking aids such as canes or walkers were not utilized in any of the TUG tests performed.

4.6 Impaired Participants

4.6.1 Lower-body Kinematics

To validate the effects of the exosuit, the lower-body kinematics of the participants for the inactive and the active conditions are compared. Participants P_1, P_2, and P_3 are provided different levels of assistance as detailed in Table I. A decrease in the knee angle of the assisted leg at the terminal swing phase is observed in all participants with varying magnitudes $P_1 = 21.22\%$ ($p = 0.0001$), $P_2 = 32.62\%$ ($p = 0.0007$), $P_3 = 34.55\%$ ($p = 0.0001$) as seen in Fig. 4.8. The three participants also present as reduction in the hip angle during the swing phase indicating reduced hip flexion when the exosuit is active. Also, for P_1 and P_3, smaller hip angles were observed during initial stance where the knee angle was also reduced. When comparing ankle angles
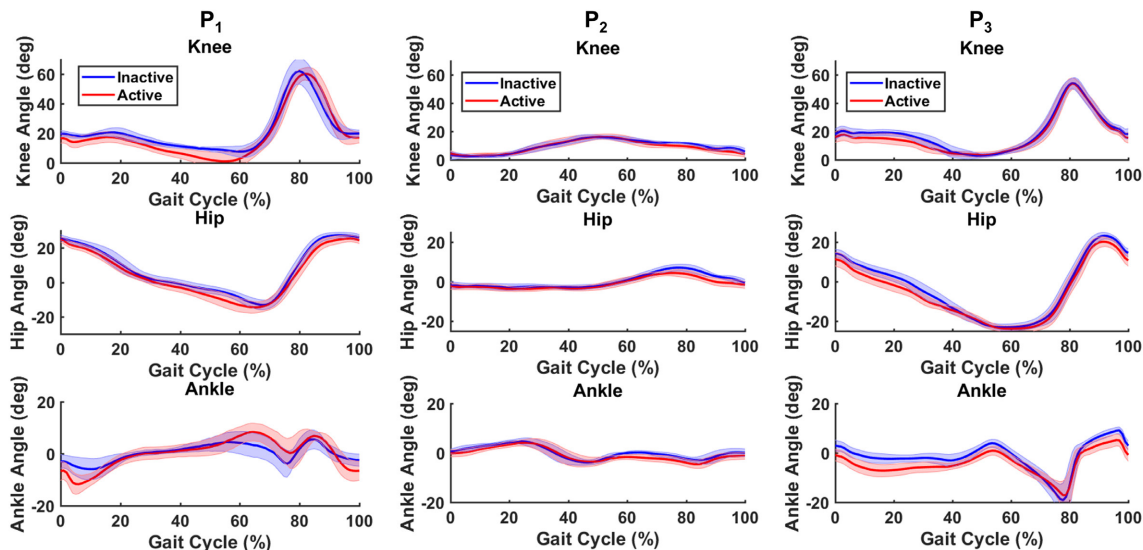
Figure 4.8 Kinematics of the Three Test Participants During Treadmill Walking for Exosuit Inactive and Active Conditions.
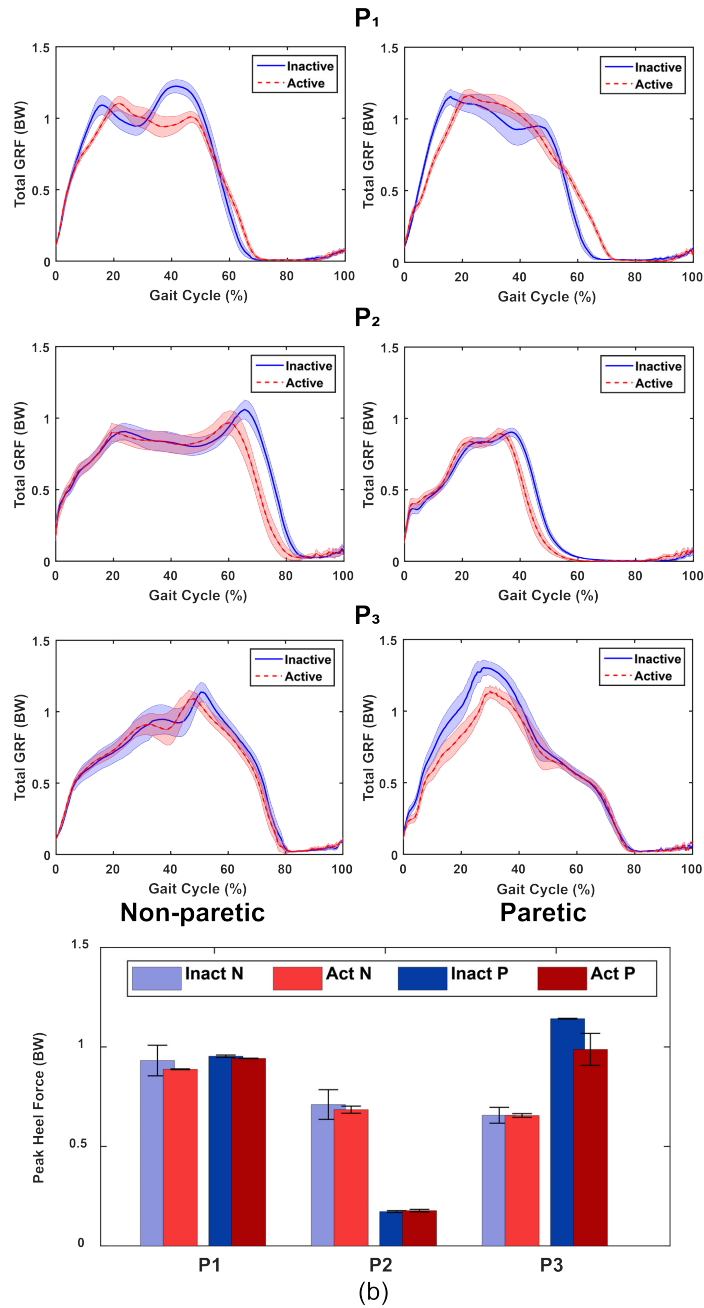
Figure 4.9 (a) Total GRF Measurements for All Impaired Participants. (b) Heel Forces for All Participants During Walking.

for the inactive and active conditions, P_1 demonstrates increased dorsiflexion during terminal stance and pre-swing whereas P_3 demonstrated decreased dorsiflexion.

4.6.2 Ground Reaction Forces

The total GRFs for the three impaired participants is as observed in Fig. 4.9(a). Decreased heel GRF is seen in P_1 and P_3 whereas P_2 presented small heel forces due to reliance on fore foot contact during initial contact, as seen in Fig. 4.9(b). It is also observed that the peak GRF on the heel is reduced by 0.16BW for P_3 ($p=0.0001$) and 0.01BW for P_1 ($p=0.084$). Only P_3 shows a statistically significant reduction on the peak heel GRF indicating a softer landing primarily due to the reliance on the treadmill handle to support himself.

4.6.3 Spatiotemporal Parameters

To examine the changes observed in the kinematics, the step length and step time for each of participant in treadmill walking were measured. As presented in Tables 4.4 and 4.5, a decreased step length (P_1=14.78% ($p=0.0001$); P_2=9.84% ($p=0.519$); P_3=7.44% ($p=0.0001$) and step time (P_1=16.82% ($p=0.0001$); P_2=6.87% ($p=0.0001$); P_3=4.84% ($p=0.0001$) were observed when the exosuit is active for treadmill walking.

Table 4.4 Step Length (mm) During Exosuit Inactive and Active Conditions of Treadmill Walking for the Three Impaired Participants.

	Left (Non-Paretic)		Right (Paretic)	
	Inactive	Active	Inactive	Active
P_1	488±27.97	421.1±17.46*	520.2±21.59	443.3±26.28*
P_2	188.1±15.91	173.7±34.18*	109.4±49.11	98.64±45.24
P_3	575.7±18	523.7±29*	613.1±32	567.5±31*

Table 4.5 Step Time (s) During Exosuit Inactive and Active Conditions of Treadmill Walking for the Three Impaired Participants.

	Left (Non-Paretic)		Right (Paretic)	
	Inactive	Active	Inactive	Active
P_1	3.38±0.06	2.81±0.03*	3.33±0.14	2.77±0.15*
P_2	1.44±0.05	1.36±0.07*	1.31±0.35	1.22±0.36*
P_3	3.71±0.1	3.57±0.1*	3.72±0.1	3.54±0.18*

4.6.4   Circumduction and Hip-hike

Compensatory hip hiking and circumduction were measured for the exosuit inactive and active conditions for all impaired participants. The distance between the ankle marker's position during stance and its maximum lateral position during swing as measured to determine the hip-circumduction during each gait cycle. A schematic
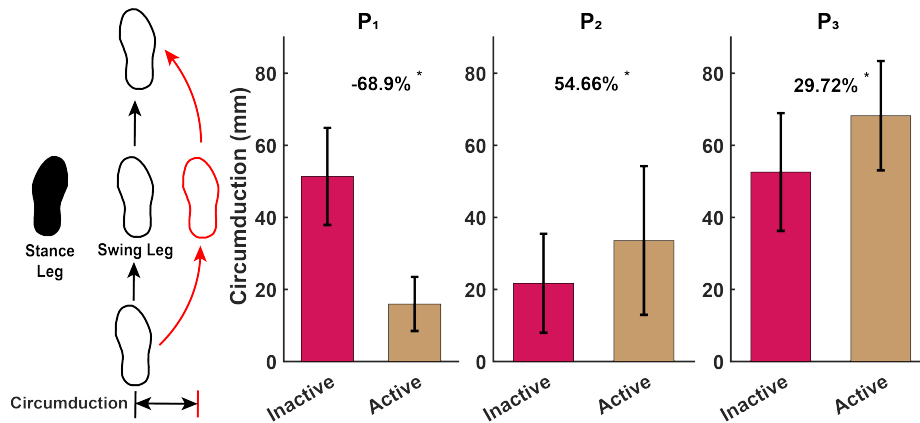
Figure 4.10 Left: Schematic Depicting Ankle cCrcumduction During the Swing Phase. Right: Hip Circumduction During Walking for P_1, P_2, and P_3 With Exosuit Inactive and With Exosuit Active. A Reduction of 68.9% is Seen in P_1 Whereas an Increase of 54.66% and 29.72% is Observed in P_2 and P_3 Eespectively. * Indicates $p < 0.05$.
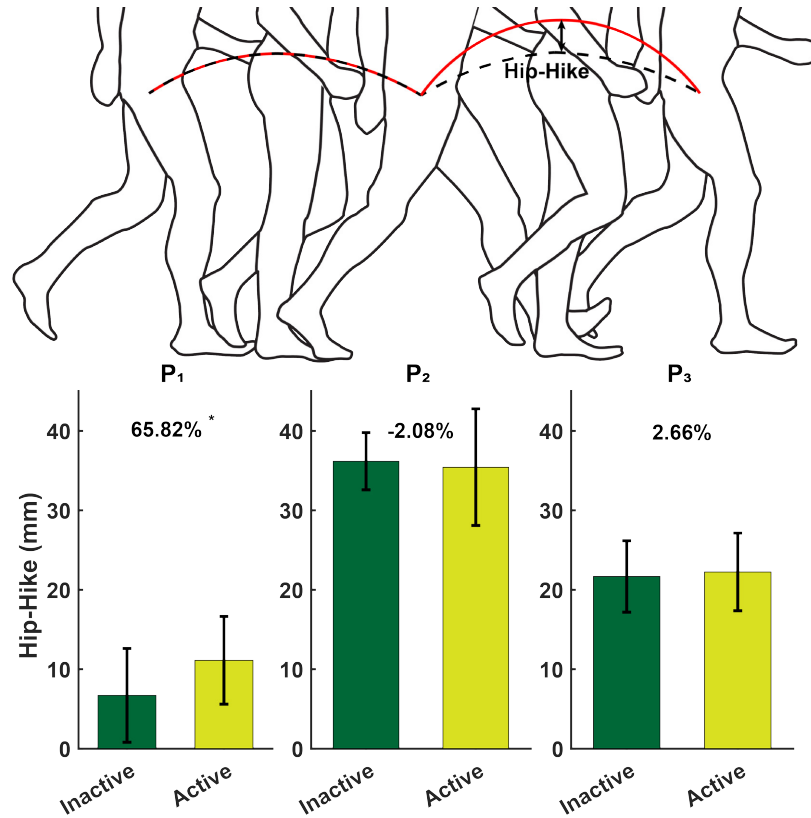
Figure 4.11 Top: Schematic Depicting Hip-Hiking During a Gait Cycle. Bottom: Hip-Hiking During Walking for P_1, P_2, and P_3 With Exosuit Inactive and With Exosuit Active. An Increase of 65.82% and 2.66% is Seen in P_1 and P_3 Respectively. A Decrease of 2.08% is Observed in P_2. * Indicates $p < 0.05$.

of the circumduction is depicted in Fig. 4.10. The hip-hike was measured using the anterior superior iliac spine (ASIS) marker as a reference point. The maximum height of the ASIS marker during the swing phase was compared to its position during standing to determine the amount of hip hiking. A schematic of the hip hiking is depicted in Fig. 4.10.

As depicted in Fig. 4.10, decreased circumduction in P_1 (p=0.0001) is observed whereas a significant increase is seen for P_2 (p=0.0302) and P_3 (p=0.0001). A significant increase in hip hike is observed in P_1 (p=0.0001) whereas no change is observed
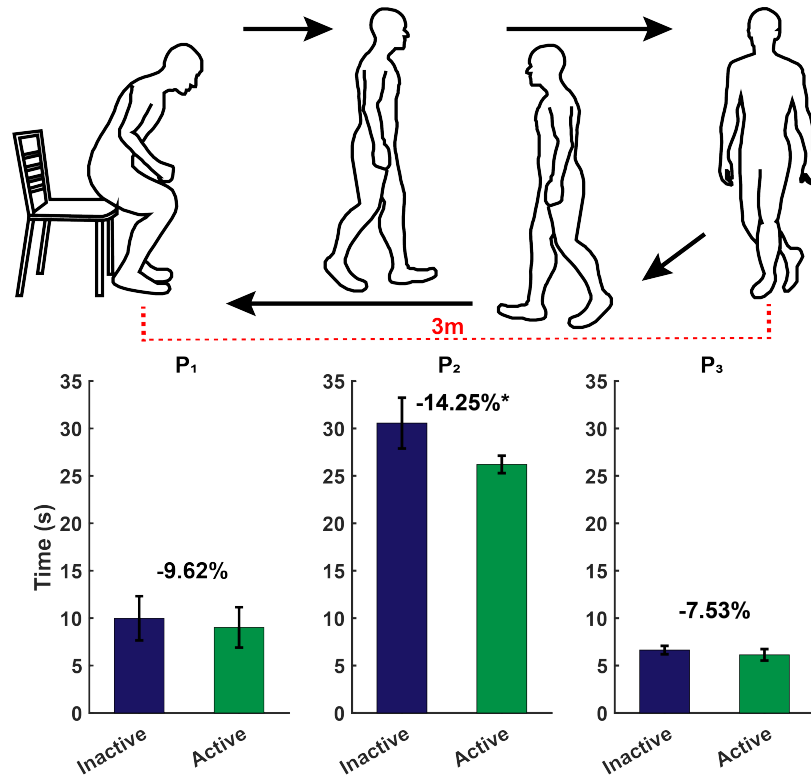
Figure 4.12 TUG Time for the Three Impaired Participants Depicting Reduction in Time With the Exosuit Active. A Reduction of 9.62%, 14.25%, and 7.53% in P_1, P_2, and P_3 Respectively.* indicates $p < 0.05$

in P_2 (p=0.2778) and P_3 (p=0.4856) as seen in Fig. 4.11.

4.6.5   Overground Walking and Timed Up and Go

Decreased TUG execution times were observed when the exosuit was active compared to the exosuit inactive condition. Participants P_1, P_2, and P_3A demonstrated a reduction of 9.62% (p=0.2579), 14.25% (p=0.0073), and 7.53% (p=0.1441) respectively as depicted in Fig. 4.12.
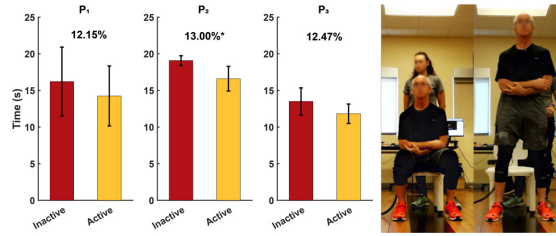
Figure 4.13 STS Timings for the Three Impaired Participants Depicting Reduction in Time for Exosuit Active Trials. A Reduction of 9.62%, 14.25%*(p=0.0073), and 7.53% in P_1, P_2, and P_3 Respectively.

4.6.6 Five Time Sit-to-Stand Transfers

A five time sit-to-stand (5xSTS) transfer test is performed to assess the functional mobility of each of the participant in addition to walking tests. A decrease in execution time is expected when using the soft exosuit due to the extension assistance provided by the device.

The impaired participants are called to start seated on a chair of 43cm height with arms crossed. Standing up from the seated position and back to the seated position is considered as one complete transfer. A total of five consequent transfers are performed and the time taken to complete the task is recorded. The physical therapists assisting in performing the test sessions are located next to the test participant to provide stability when the participant loses balance and do not interfere with the activity otherwise. A decrease of 12.15%, 13.00%*(p=0.038), and 12.47% is observed in P_1, P_2, and P_3 respectively when the exosuit is active as seen in Fig. 4.13.

4.7 Discussion

The soft inflatable exosuit was applied to seven healthy participants to study the effects of knee extension assistance in the swing phase. Reduced knee angle at terminal swing was presented by six out participants when the exosuit was active. Varying

sEMG patterns for the exosuit active condition were observed when compared to non-assisted trials. The diversity in the sEMG patterns can be attributed to individual muscle responses during walking for each participant. Overall, a significant reductions in the quadriceps for a large number of participants (VM, n=6; RF, n=4; VL, n=3) when the exosuit is active and assisting. All participants demonstrated varying heel forces when the exosuit was active.

This study sought to explore the effects of knee extension assistance in the swing phase and initial stance for participants undergoing post-stroke rehabilitation. The kinematics of three participants is examined during treadmill walking. Reduced terminal-swing knee angle was demonstrated by the three impaired participants when knee extension assistance was provided by the exosuit. Reduced hip flexion angle for all participants was also observed when knee extension assistance during the swing phase and initial stance was provided. Reduced hip and knee angles were seen in P_1 and P_3 during the stance phase. The reduced knee angle during initial stance could be an effect of the additional knee stiffness provided by the exosuit during initial contact. The reduced hip angle during the swing and the stance phase could potentially be caused as a compensation to the knee extension assistance provided by the exosuit. For safety concerns, all impaired participants gripped the treadmill handle during treadmill walking. Therefore, a total GRF lower than the BW is observed in P_2 the support provided by the handrail. This reliance on the handrail could also partially lead to the diverse results for the rest of the impaired participants where P_1 shows a small decrease and P_3 shows a significant reduction in peak heel force.

Spatio-temporal parameters such as step length and step time were aso studied to examine cadence of walking. A reduction in step length was observed for all impaired participants which could be caused due to the reduced hip flexion angle during the swing phase. Additionally, reduced step time was also observed. The reduction in

step time indicates faster stepping speed walking implying higher cadence during treadmill. A possible reason could be the use of a modified gait strategy to maintain a constant walking speed at the treadmill with a higher cadence induced by the knee extension assistance.

The compensatory gait patterns such as circumduction and hip hiking when using the exosuit were also studied. P_1 demonstrated large reduction in hip circumduction with increased hip hiking while walking. P_2 and P_3 demonstrated reduced hip circumduction and no change in hip hiking during a gait cycle. Prior work suggests that the inability to clear the ground during walking is a combination of inadequate knee flexion and ankle dorsiflexion during the swing phase [70]. Analysis of knee flexion indicated that the maximum knee flexion angle during a gait cycle was not altered by the assistance provided. Therefore, the increased circumduction observed in P_2 and P_3 can be attributed to reduced hip flexion during the swing phase causing increased leg length which promotes the use of the compensatory gait pattern [71]. The increased hip hiking can also be attributed to the increased leg length during swing phase as observed in P_1.

A reduced TUG execution time was seen in all three impaired participants. Only P_2 demonstrated a statistically significant change in the execution time. Participants P_1 and P_3 executed the test within $10s$ which is considered as normal completion time by Lysack et. al [72]. The reduced TUG times seen using the exosuit, although smaller than the smallest real difference metric formulated by Flansjber et. al. [73] provided promise of use of such systems in wearable devices.

The 5xSTS test is performed to assess the functional mobility of the three test participants. A reduction in 5xSTS times is observed in all participants when the exosuit is active pointing to evidence of potential use in day to day activities requiring knee extension assistance.

Chapter 5

THE DESIGN OF AN UNTETHERED SOFT INFLATABLE EXOSUIT USING
INFLATABLE ACTUATOR COMPOSITES AND A PORTABLE PNEUMATIC
SOURCE

The previous three versions of the inflatable exosuit utilized inflatable actuators
tethered to an off-board air compressor which limited the usage of the exosuit to
lab settings. Additionally, due to the internal volume of the inflatable actuators, the
actuation speed of the exosuit was limited. Therefore, to improve the performance
of the exosuit to facilitate faster inflation speeds as well as to allow for outdoor
applications, this chapter focuses on the design of inflatable actuator composites that
effectively reduce actuator volumes with the same performance. Also, the design of a
portable pneumatic source to allow for outdoor operation of the wearable system is
presented. The major contributions of this chapter are as follows -

- The design of a soft-rigid hybrid inflatable actuator composite with reduced
  internal volume resulting in lower cost of actuation and higher.

- The design of a portable pneumatic source capable of generating high pressure
  and flow outputs.

- Integration of the inflatable actuator composites and the portable pneumatic
  source into an untethered soft inflatable exosuit.

- evaluation of the untethered exosuit with three healthy participants while walk-
  ing on an incline.

5.1 Inflatable Actuator Composite

5.1.1 Motivation

To design energy-efficient inflatable actuators using fabrics, it is critical to study the energy balance of inflatable systems. Work on computing the efficiency of elastomeric systems using the energy balance principle and port-hamiltonian theory has been attempted [74]. Several works have attempted to study inflatable beams and their buckling using structural mechanics [75]. Work of inflatable pneumatic interference actuators attempted to study performance estimation of such actuators using virtual work principle [76]. Despite several attempts at the design of inflatable beams and actuators, limited literature on energy balance of inflatable systems is available.

Therefore, in this chapter, we study the energy in and out of the system to aid in designing more efficient actuators. The design of inflatable actuator composites focuses on reducing actuated volumes by adding rigid inflatable sections. Hence, this work attempts to lay the foundation for understanding the energy balance of inflatable actuators fabricated using isotropic film based materials such as TPU and fabrics.

Mechanical work in general can analyzed using the following equation

$$E_{in} = E_{stored} + E_{useful} + E_{lost}, \tag{5.1}$$

wherein, E_{in}, E_{stored}, E_{useful}, and E_{lost} are the energy input, stored energy, useful energy, and energy loss, respectively.

In pneumatic systems, input work is provided in the form of pressure and flow which can be computed by using the following equation

$$E_{in} = \int P dV. \tag{5.2}$$

where P is the internal pressure and dV symbolizes the change in volume of the system.

Losses in mechanical systems can be attributed to factors such as friction and hysteresis.

$$E_{lost} = E_{leak} + E_{friction} + E_{hysteresis} \tag{5.3}$$

Since it is often difficult to compute energy losses due to friction and theoretically we can assume that there are negligible leaks in the system, energy lost from the system can be narrowed down to

$$E_{lost} = E_{hysteresis} \tag{5.4}$$

The energy stored in inflatable beams and membranes is dependent on the strain energy of the material utilized to fabricate them. The strain energy stored in any material can be determined by

$$E_{Stored} = \frac{1}{2}kx^2 \tag{5.5}$$

where, k and x are the material modulus and strain respectively.

Films and fabrics typically used to design these actuators do not have an inherent compressive stiffness. They generate reactive forces under tensile loads. This work utilizes inflatable actuators fabricated using isotropic fabrics such as nylon with high material modulus k. Prior work on soft pneumatic actuators report pressures has high as 0.7 MPa [77] which is not sufficient to strain the fabrics enough to cause elastic or plastic deformation. Therefore, we can assume that

$$E_{Stored} = \frac{1}{2}kx^2 = 0 \tag{5.6}$$

Hence, finite element and analytical models for inflatable actuators and beams could be one approach to this problem [75, 78]. The aforementioned models for inflatable beams and the energy balance indicate that the inflation work is directly proportional to the internal volume. Therefore, reducing the volume of inflatable actuators reduces the input work of the system. These improvements to inflatable actuators have also been suggested in prior work [51].
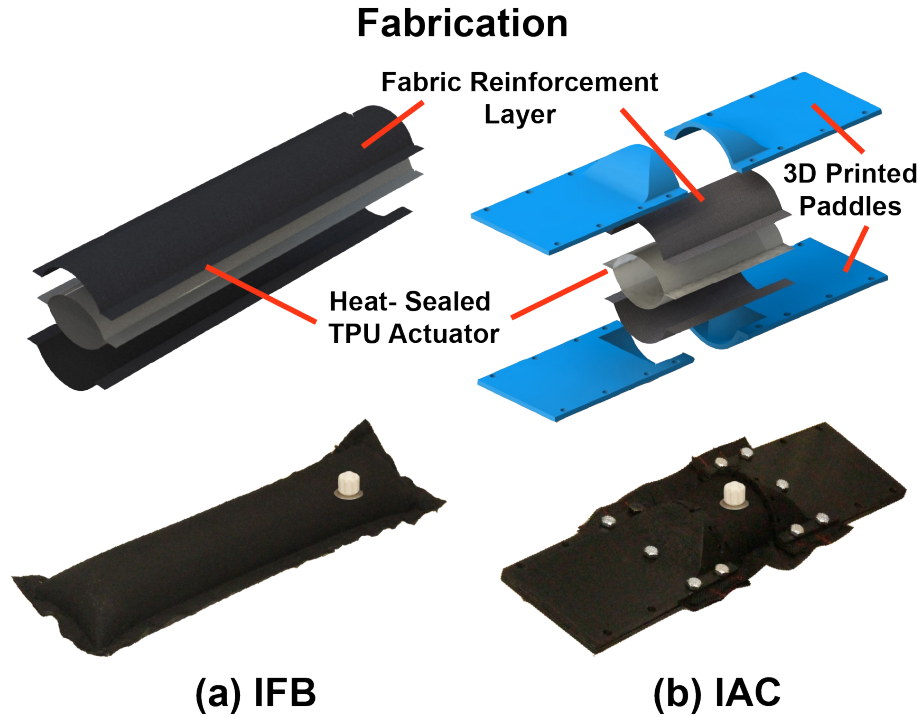
Fabrication

Figure 5.1 (a) Fabrication of the Inflatable Fabric Beam (IFB) Utilizes an Inner Heat-sealed TPU Chamber Which Is Encased in a Fabric Reinforcement Layer Which Allows for Higher Pressure Retention Capability. (b) the Inflatable Actuator Composite (IAC) Utilizes a Fabric Encased Inflatable Section Which is Smaller in Length. The Inflatable Section Is Replaced with 3D Printed Paddles That Replace a Portion of the Inflatable Volume with Rigid Components.

To fabricate the IAC, a nylon fabric encased inflatable actuator is attached to 3-D printed rigid paddles at two ends. The fabrication method for the IAC is as shown in Fig. 5.1. Two layers of TPU are layered and sealed on all for sides to create and inner bladder. The heat sealed TPU is then encased in nylon fabric which is sewn around the film. The nylon fabric allows for increased pressure retention since the TPU elastic limit is not reached. The 3D-printed paddles are attached to the ends

of the inflatable section by bolting and sewing. The 3D-printed paddles are designed with a concave shape on one end in order to account for the inflation of the fabric section. The ends of the 3D-printed paddles are made flat to reduce the overall weight of the actuator.

5.1.3   Testing of the actuators

To determine the performance of the designed IACs, the actuator was compared to the previously designed IFB. To keep this comparison fair, the fabric section of the actuators were fabricated with the same width ensuring that the cross-sectional area remains same. The difference between the actuators was the length of the inflatable section. The length of the inflatable section for the IAC was designed to the one third of the IFB in order to reduce overall volume of the actuator. For the following comparison, the inflatable section of the IAC was designed to be 33% of the IFB to demonstrate feasibility of such actuators.

The actuators were mounted to a test setup and only allowed crease at mid-point. While one end was clamped, the other end was allowed to hang under the influence of gravity. Due to the light weight of these actuators, both the IAC and IFB tend to straighten completely at low pressures without external loads. Therefore, a 1 kg mass was attached to the hanging end of the actuator for testing. As the actuators were inflated in pressure steps of 0.034 MPa, the deflection of the hanging end was measured. The maximum pressure the actuators were inflated to was restricted to 0.2760 MPa. The deflection angles against the internal pressure for the IAC and IFB are as demonstrated in Fig. 5.2. A root mean square error (RMSE) of 5.16° was obtained when the IAC was compared against the IFB.
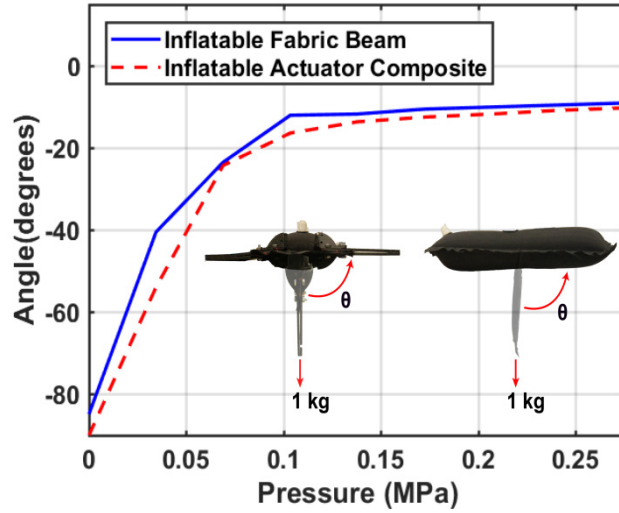
Figure 5.2 The IAC and IFB Tested in a Cantilever Beam Fashion with the Actuator Creased at the Mid-point. The Pressure is Increased in Intervals Of 0.034 MPa with Actuator Deflection Being Measured. An RMSE Value of 5.16° is Observed When Comparing the IAC and the IFB.

5.1.4   Finite Element Method Modeling

Finite element models for the IAC and IFB were created to further study the behavior of the actuators. Models for both the actuators were generated using ABAQUS (Simulia, Dassault Systemes). In order to simulate these actuators accurately, the material properties of the TPU, Nylon fabrics, and the polylactic acid (PLA) used to fabricate the actuators were collected using tensile tests as well as material properties databases (CITE PLEASE). The ASTM D882 test protocol was followed and the material properties for TPU and Nylon 40D were determined to be E=5.1 MPa, ν=0.4 and E=728.22 MPa, ν=0.35 respectively. The material properties of PLA were determined to be E=3600 MPa, ν=0.3.

Further, to model the inflatable sections of the actuators, shell elements were utilized to order to mimic the thin walled structures. A material thickness of 0.3

66
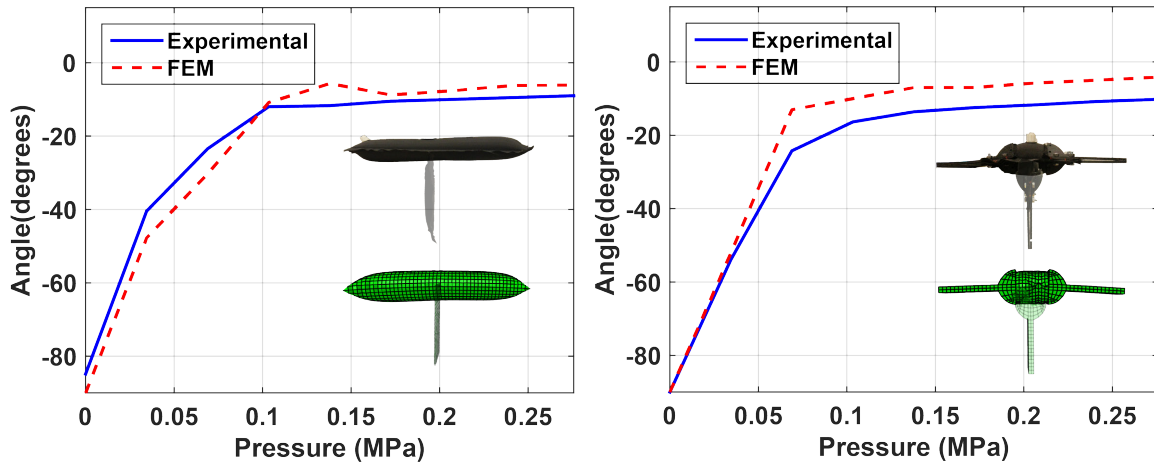
Figure 5.3 Fem Models for the IFB and IAC Validated Against Experimental Results.

mm was used for the shell elements. These simulations were created using a dynamic explicit environment to account for high material deformation during inflation. The inflatable section of the actuators was created in a similar manner to the fabrication. Two layers of the films were placed on top of each other and the heal seals and stitches were designed using tie constraints. To further design the 3D-printed paddles, the PLA was modeled using solid elements due to the material having relatively higher mass compared to the thin films. A simplified model of the 3D-printed paddle was created in the simulation environment and attached to the inflatable section using tie constraints. The ends of the actuators were fixed in space using boundary conditions similar to the experimental setup.

The 1 kg load was added to one end of both the actuators to simulate the added weight. The IFB was designed bent at the mid point due to the simplified shape of the actuator. This was not possible in the case of the IAC due to the interaction between the PLA paddles. Therefore, an additional step to influence the actuator to bend to the initial position was added for this simulation. A pressure load was added to the shell elements to create actuator inflation. The pressure versus deflection was measured throughout the inflation process. Quasi-static condition was maintained

67
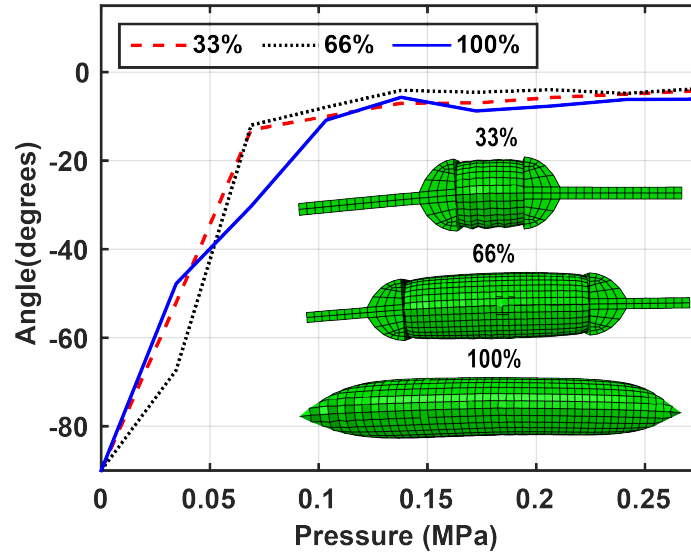
Figure 5.4 FEM Simulations for IACs with 33% and 66% Internal Volume as Compared to the IFB. Both of the IACs and the IFB Demonstrate Similar Pressure-Deflection Characteristics.

during the simulation to remove the influence system dynamics during measurement. The measured and simulated deflections compared as seen in Fig. 5.3. The models for the IFB and the IAC demonstrated RMSE errors of 4.63° and 6.33° respectively. The differences between the models and the experimental results were attributed to errors in fabrication as well as losses during experimentation.

To analyze the effect of volume of the inflatable section on the IAC, FEM models of IACs with varying volumes were created. Models for the IACs with inflatable sections of 33% and 66% volumes of the IFB were created. The pressure versus deflection profiles for the two IAC models and the IFB were compared as shown in Fig. 5.4. The three FEM models present similar behavior demonstrating that volume does not have an effect on the actuator performance. In order to explain these results we look to work by Nesler et al. [76] which presented a model for these type of actuators. The model presented by the aforementioned group demonstrated that the actuator

68
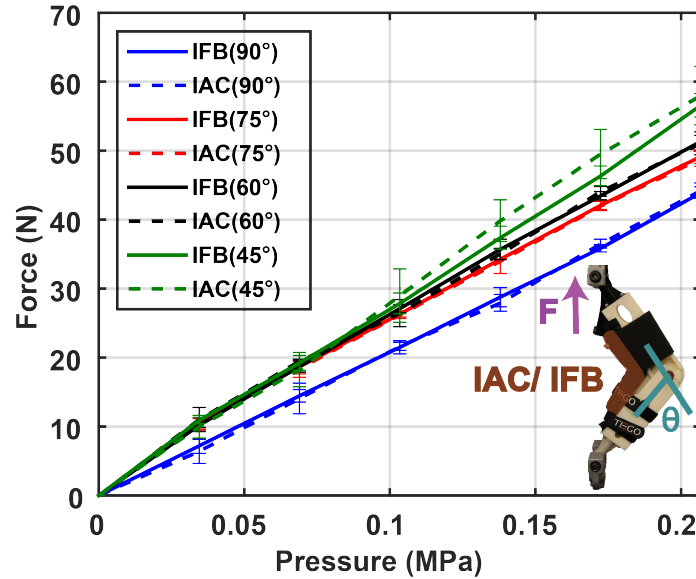
Figure 5.5 Force Output of the IAC and IFB When Mounted on an Analog Leg Attached to a UTM. The IAC and IFB Both Demonstrate Identical Force Outputs at a Constant Angle.

performance is dependent on the creased volume and not the overall actuator volume. In this work, we restrict the simulation volume of the IAC to 33% since the 3D-printed paddles would make contact if the volume of the inflatable section is reduced further.

5.1.5   Actuator Testing

To examine the force output of the IAC and compare it with the IFB, the actuators were mounted on to the analog leg joint. The actuators were placed in a pouch behind the knee joint which was mounted on a universal testing machine. When inflated, the actuators would apply a torque to the knee joint which was measured in the form of a force transmitted to the load cell mounted on the UTM. The test setup is as shown in the inset of Fig. 5.5. The flexion angle of the joint was varied and the force output for the IAC and IFB were measured for 45°, 60°, 75°, and 90°. The actuators were inflated and quasi-static force measurements were recorded. From Fig. 5.5, the
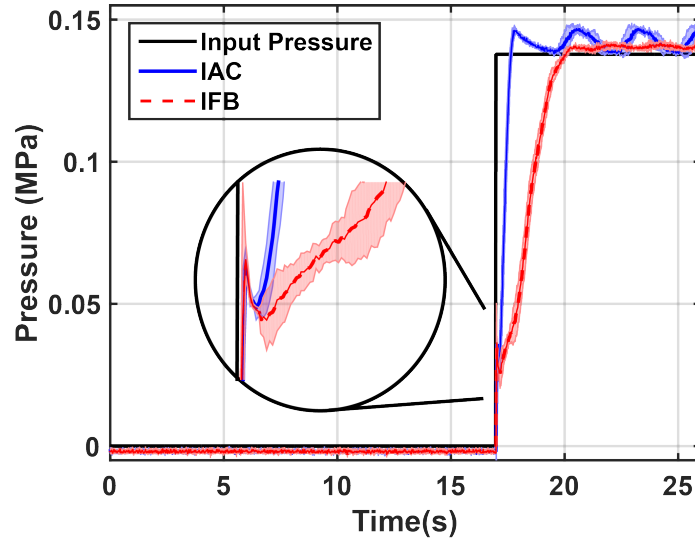
Figure 5.6 Pressure Step Response of the IAC and IFB When Connected to the Same Pressure Source. The IAC Inflates Faster than the IFB Owing to the Reduced Volume.

IAC and IFB demonstrated similar force outputs which further aligns with the model result presented by Nesler et. al. [76].

Since less energy is used to actuate the IACs due to reduced volume, the rise time of the composite was compared to that of the IFB. A air source with a pressure and flow of 0.138 MPa and 100 $SLPM$ respectively was connected to the IAC and IFB. A solenoid valve was used in series with the pressure source and the actuators to trigger inflation. Once the valve was turned on, the actuators would inflate to maximum pressure while the response time was measured.

As seen in Fig. 5.6, the IAC and IFB reached a maximum pressure in 0.68 s and 3.08 s, respectively. These results demonstrated that the step response time for the IAC was 4.5 times greater than the IFB. The IAC was expected to inflate faster than the IFB due to the reduced volume and energy cost for actuation. Further, a pressure spike was observed as soon as the valves were opened due to the system dynamics of the pressure regulator and valves. These pressure spikes were also observed in work presented by Chung et. al. [51]. Both overshoot and fluctuation are observed in the

70
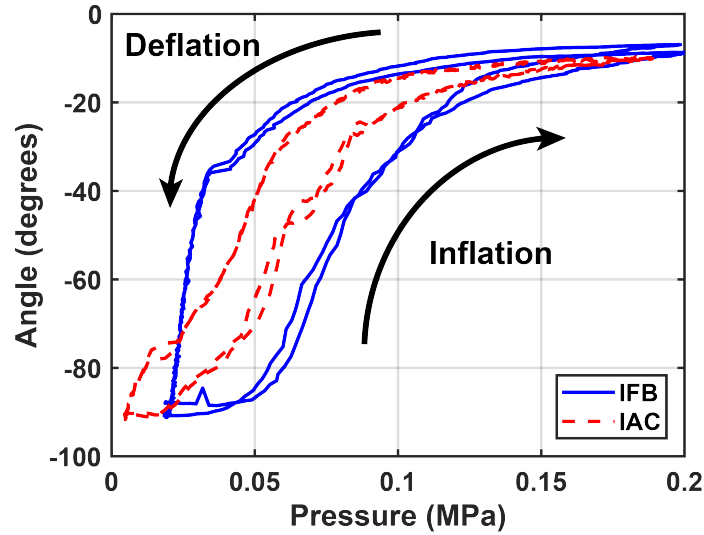
Figure 5.7 Hysteresis Observed in the IAC and IFB During Inflation and Deflation. The IAC Demonstrates Lower Hysteresis as Compared to the IFB.

pressure profile of the IAC due to the pressure regulator dynamics.

The hysteresis in actuator deflection during the inflation and deflation of the IAC and IFB was analyzed. The actuators were set up in a similar manner to the pressure-deflection experiment with a $1kg$ weight attached to the overhanging end. A linear pressure input ($0.028\ MPa/s$) was provided to the actuator wherein the pressure was increased to $0.2\ MPa$ and then decreased to $0\ MPa$. As seen in Fig. 5.7, both the IAC and IFB show hysteresis during dynamic inflation and deflation. The hysteresis observed in the IAC and IFB were compared by computing the are inside the curve. The area for the IFB was 54.48% larger than that for the IAC indicating that more energy is lost during the actuation of the IFB.

71

5.2 Design of a Portable Pneumatic Source

5.2.1 Design and Fabrication

In order to design an actuation unit to power the exosuit, a portable pneumatic source capable of generating high flow and pressure outputs is required. This is due to the inflation volume of the IFBs which require approximately 0.25 L of compressed air for complete inflation [66, 67]. Therefore, in order to actuate the two IFBs in the previous version of the exosuit, a pneumatic supply capable of generating 60 $SLPM$ and 0.027 MPa is required. With the design of the IACs used in the exosuit, the flow requirement is reduced to 20 $SLPM$ due to the volume of the actuator being 33% of the IFB. Further, the weight and size of the pneumatic actuation unit has to be restricted to allow for we arability. Therefore, the functional requirements for the portable pneumatic source were set as listed in Table 5.1.

Past work on inflatable devices utilized pneumatic compressors, micropumps, and a slider-crank based [79]. The use of air compressors to power inflatable robots limits such robots to indoor and tethered applications. Further, commercially available pneumatic micropumps do not provide both high flow and pressure outputs to actuate wearable systems. The portable source designed by Kim et. al. [79] is capable

Table 5.1 Requirements of the Portable Pneumatic Source Based on Previous Versions of the Exosuit.

Characteristic	Requirement
Weight	$< 5kg$
Maximum pressure	0.140 MPa
Maximum flow rate	20 $SLPM$
Dimensions	$< 20cm \times 20\ cm \times 12.5\ cm$

of generating high pressures is not able to generate the aforementioned flow of 20 $SLPM$. Therefore, it is critical to design a customized portable pneumatic source for our application.

The working principle of the portable pneumatic source utilized a lead screw mechanism which drives a double acting pneumatic cylinder coupled to it. A DC motor was used to drive the lead screw clockwise and counter-clockwise. The outputs
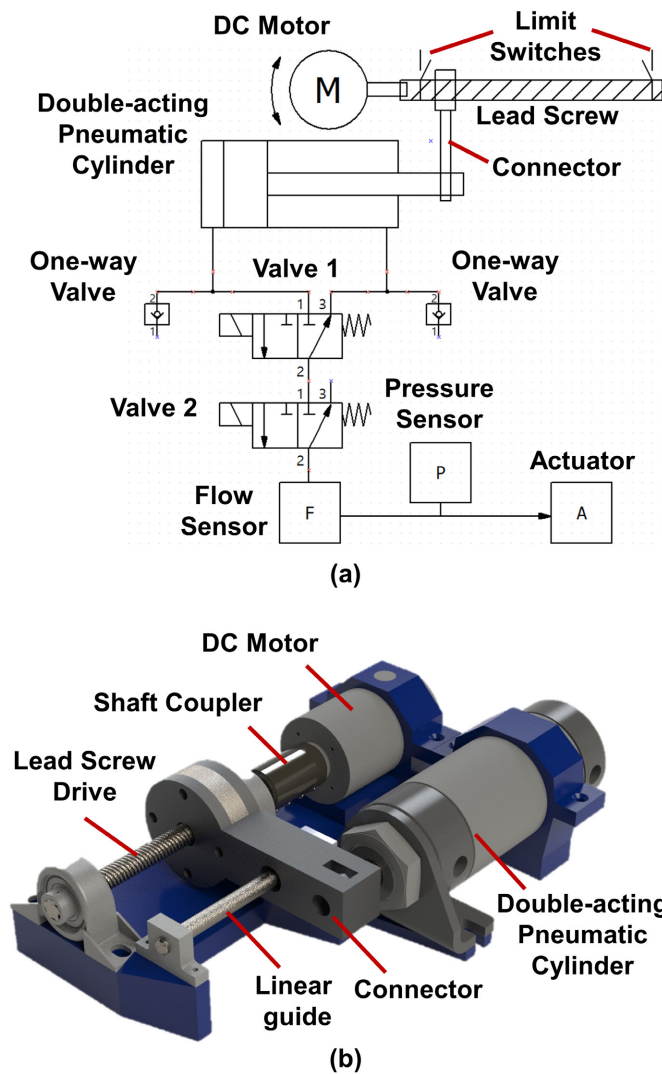
Figure 5.8 (a) Electropneumatic Schematic of the Portable Pneumatic Source. (b) 3D Rendering of the Portable Pneumatic Source.

of the pneumatic cylinder were connected to solenoid valves which diverted the flow of air during operation. The valves were set up in a manner that when air from one chamber of the cylinder was being forced out, the other chamber sucked in air. The schematic of the complete system is as shown in Fig. 5.8(a).

To fabricate a system as shown in the schematic 5.8(a), a CAD model taking inspiration from the slider-crank mechanism as well as reciprocating piston pump, a portable system was designed as shown in Fig. 5.8(b). A base was designed and fabricated using 3D-printed nylon material to mount the lead crew mechanism, motor (Amp-flow A23-150, 24V 10A), and pneumatic cylinder (bore=3.175 cm, stroke=6.35 cm). The lead screw as supported on both ends using bearings and coupled to the DC motor using a shaft coupling. The lead nut of the the linear drive mechanism was attached to the double acting pneumatic cylinder. A custom coupler was utilized in order to do so. The coupler was supported using a linear bearing to ensure mechanism alignment. It is noted that a gearbox is not utilized in this portable source to reduce the weight of the overall system. Also, the use of the lead screw mechanism minimizes the height profile of the portable source.

The DC motor is controlled using a micro-controller (Raspberry Pi 3) and a motor driver (30A 5-30V Single Brushed DC Motor Driver, Cytron). The rotation direction of the motor are controlled using limit switches which are attached at the ends of the lead screw. At the end of every stroke of the pneumatic cylinder, the lead nut comes into contact with the limit switch and the direction of motor rotation is reversed. 3-port 2-way Solenoid valves (MHE3-MS1H valves, Festo, Hauppauge, NY) and one way check valves are attached to the cylinder outputs to modulate air path during operation.
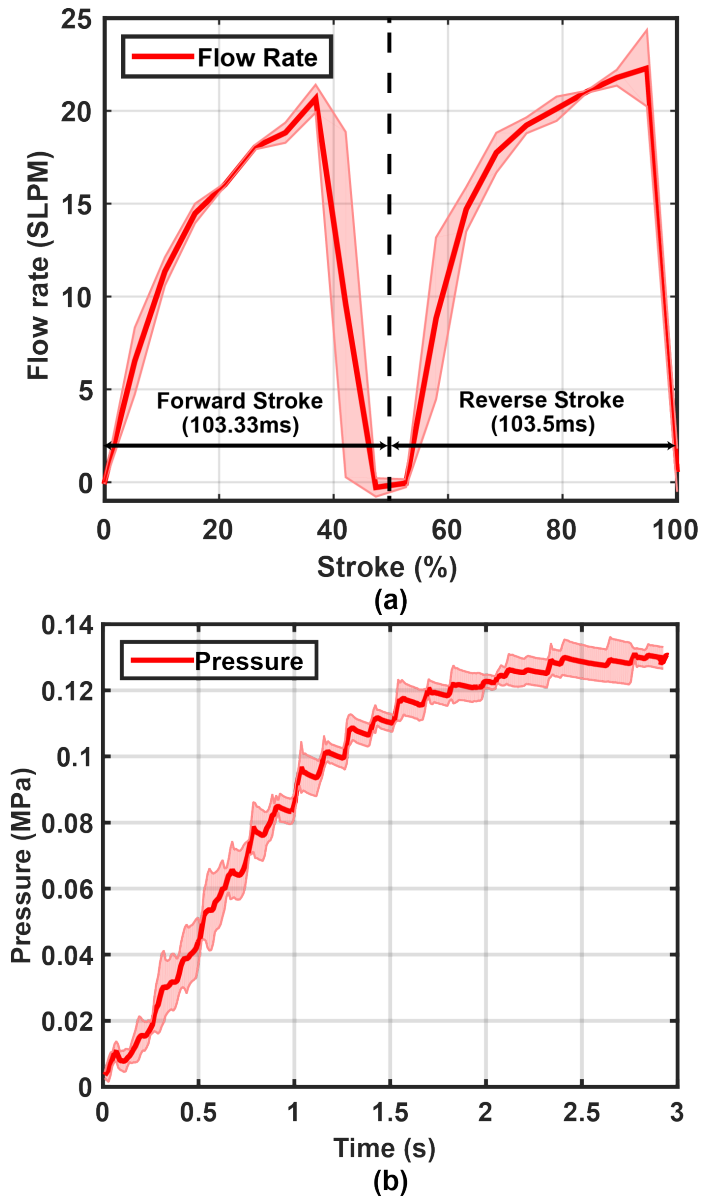
Figure 5.9 (a) Flow Output of the Portable Pneumatic Source. (b) Maximum Pressure Output of the Portable Pneumatic Source.

5.2.2   Testing of Pressure and Flow Rates

To measure the pressure and flow outputs of the portable pneumatic source, sensors were attached to the output of the system. To measure the maximum pressure generated by the pneumatic source, a pressure sensor (ASDXAVX100PGAA5, Honey-

well International Inc., Morris Plains, NJ) and an IAC were connected to the output. The portable source was allowed to operate until the motor stalled. In this way it was ensured that the system achieved its maximum possible pressure output over multiple strokes of the pneumatic cylinder. A maximum pressure of 0.131 MPa was achieved using the portable source as seen in Fig. 5.9(b).

To measure the flow output of the portable pneumatic source, a flow sensor (HA-FUHT0050L4AXT, Honeywell International Inc., Morris Plains, NJ) was attached to the output. The flow rate was measured for both the strokes of the pneumatic cylinder. As seen in Fig. 5.9(a), the portable system generated varying flow rates for the forward and reverse strokes. This was due to misalignment in the linear drive mechanism caused to fabrication tolerances. Overall, an averaged flow rate of 21.45 $SLPM$ was generated using the portable pneumatic source.

The comparison of the portable pneumatic source with some commercially available micropumps is as listed in Table 5.2. The portable pneumatic source designed in this work is capable of producing both high pressure and flow outputs as compared to commercially available air pumps with similar outputs.

Table 5.2 Pressure and Flow Outputs of Commercially Available Pneumatic Pumps Benchmarked Against the Presented Portable Source.

Pneumatic Pump	Pressure	Flow rate
This work	0.131 MPa	21.45 $SLPM$
TOPSFLO TM40A-A [80]	0.18 MPa	10 $SLPM$
KNF NMP 850 [81]	0.151685 MPa	8 $SLPM$
Parker BTX-Connect [82]	upto 0.2 MPa	upto 11 $SLPM$
Binaca GX series [83]	upto 0.117211 MPa	upto 17 $SLPM$

5.3   Integration of the Portable Exosuit System

For use with the soft inflatable exosuit, the portable source was mounted onto a backpack frame. An acrylic board was utilized to mount the portable pneumatic source, the electronics (micro-controller, power circuit, and motor driver), and solenoid valves were mounted on to the board. A lithium polymer battery was utilized to power the pneumatic source and the electronic components. The system is as depicted in Fig. 5.10(a). The complete system mounted on the backpack weighed 5.1 kg with all the components. This system would be carried by the user when wearing the exosuit.

The IACs were integrated into a knee sleeve to provide knee extension assistance. As discussed in the previous chapters, the IACs were placed behind the knee joint at the popliteal fossa. The IACs were stitched onto the sleeve using fabric pouches and sewing thread. Hook and loop straps were utilized to attach the knee sleeve to the leg. The straps allow for transfer of forces from the IACs to the leg by creating tension, straightening the knee joint. The rigid paddles of the IAC were padded using foam to interface the 3D-printed parts to the soft muscle tissue. Similar to the previous versions of the exosuit, the IACs inflate to provide assistance to the quadriceps. The knee sleeve, two IACs, and straps all together weighed 295 g which was the total mass of the exosuit on the knee and is depicted in Fig. 5.10(b).

For gait detection, smart shoes [84, 85] were were integrated with electropneumatics and utilized. For this work, the assistance was provided to the stance phase of incline walking. A simple control method where the exosuit was allowed to inflate at heel strike and deflate at toe off was used. The during inflation, the actuators would provide assistance to the quadriceps during weight transfer to the leg.

For this incline walking study, three healthy test participants with the anthro-
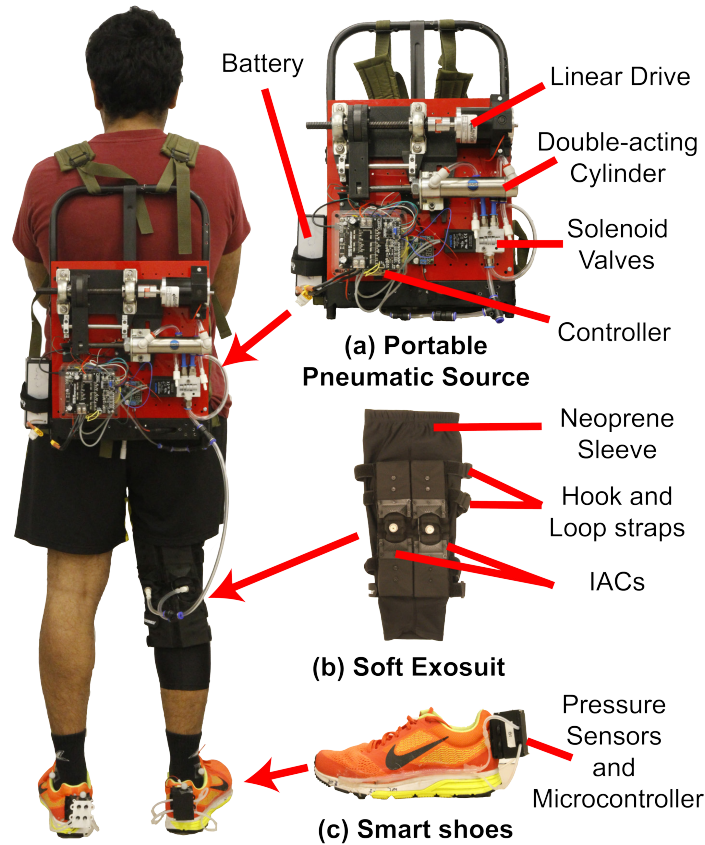
Figure 5.10 The Untethered Version of the Exosuit As Worn by a User. (a) Backpack Frame With the Portable Pneumatic Source and Electropneumatic Components Mounted on an Acrylic Board. (b) Soft Inflatable Exosuit Designed Using a Neoprene Interface With the Iacs Mounted on the Back of the Leg. (c) Smart Shoe Insole Sensors for Gait Feedback.

pometric data reported in Table 5.3 were recruited. The participants walked on a treadmill set at a $5°$ angle and a speed of $0.3m/s$ for a time interval of one minute. The muscle activity of the Vastus Lateralis (VL) muscle group was examined during incline walking. Other muscles of the quadriceps were not examined since this work was a pilot study to evaluate feasibility of inflatable exosuit systems for incline walking. The walking trials were performed for three conditions - Baseline (no exosuit), Inactive (exosuit worn but not assisting), and Active (exosuit worn and assisted). The collected sEMG data was rectified and filtered using a moving average filter. The data

Table 5.3 Height, Weight, and Age of the Recruited Test Participants. All Participants Recruited for This Test Were Male.

	Height	Weight	Age
P_1	170 cm	78 kg	27
P_2	165 cm	78 kg	25
P_3	177 cm	74 kg	24

is normalized to maximum voluntary contraction to compare results between individual participants. The area under the curve for the filtered and normalized sEMG was used for comparison.

The muscle activity of the Vastus Lateralis for all participants is as shown in Fig. 5.11. When the muscle activity for the Baseline and Inactive conditions were compared, an increase was observed. The muscle patterns were also shifted towards the right for the Inactive condition. This was due to the added weight of the portable source mounted on the backpack. When comparing the exosuit Active with Baseline, a reduction in muscle activity was seen for all participants but the muscle response remained shifted due to additional weight on the body. The reduced Vastus Lateralis
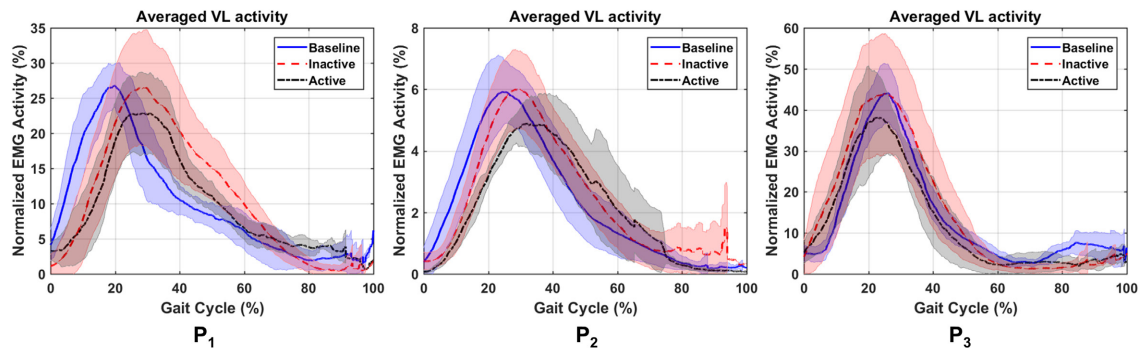
Figure 5.11 VL Activities for the Three Participants During Incline Walking Averaged over One Minute for the Baseline, Inactive, and Active Conditions.

Table 5.4 VL Activity When Comparing Baseline with Inactive and Baseline with Active Trials. + and - Indicate an Increase and Decrease in Muscle Activity Respectively.

	P1	**P2**	**P3**
Baseline vs Inactive	+8.94%	+4.75%	+7.32%
Baseline vs Active	-3.31%	-7.89%	-10.92%

muscle activity demonstrated feasibility of use of such systems for human augmentation.

Chapter 6

CONCLUSIONS AND FUTURE WORK

6.1 Conclusion

This work presented the design, control, and evaluation of a soft-inflatable exosuit for knee extension assistance. Several versions of the exosuit with subsequent design iterations and their evaluation with human test participants were presented.

The initial version of the exosuit utilized inflatable actuators of I cross-section fabricated using heat sealed TPU. The inflatable actuators were characterized to generate $4.4Nm$ of torque at $60°$ which is equivalent of 25% of the knee extension torque during the swing phase. The inflatable actuators were integrated into a neoprene knee sleeve utilizing nylon fabrics with hook-and-loop straps. An FSR based insole sensor was designed to obtain gait phase information for heel-strike and toe-off. The exosuit was controlled to inflate at toe-off when the swing phase was detected. The exosuit was tested with one healthy test participant demonstrating a 7% reduction in VL activity during walking.

Improving upon the previous version of the exosuit, the second version of the inflatable exosuit was designed. For better quality gait phase information, smart shoe insole sensors as well as IMUs were integrated into the exosuit. Improvements to the inflatable actuators were also implemented by utilizing bigger pneumatic ports for better flow characteristics as well as a dedicated port for pressure sensing. The quasi-stiffness of the human knee joint was modeled using experimental data obtained from a healthy participant. The inflatable actuator stiffness was also characterized for angles ranging from $10°$ to $60°$. A high-level controller was designed to calculate

the desired stiffness utilizing knee angle and shoe feedback using the human stiffness model and actuator stiffness model. A low-level controller was designed to modulate the valves to achieve the desired pressure generated by the high level controller. The exosuit was tested with 3 healthy participants examining knee extensor and flexor muscle activity. A reduction in the quadriceps activity with an increase in the hamstring activity was observed.

A third version of the inflatable exosuit was designed in order to generate $24Nm$ of knee extension torque. This exosuit was applied to seven healthy participants to further examine effects of knee extension assistance during the swing phase. The knee kinematics, sEMG activity, and ground reaction forces were analyzed. The exosuit was also applied to three impaired participants undergoing post-stroke physical therapy. For the impaired participants, the knee kinematics, ground reaction force, spatiotemporal parameters, hip hike, circumduction, and timed up-and-go test. Reductions were observed in 1) overall muscle activity of quadriceps in healthy participants, 2) terminal-swing knee angles in healthy and impaired participants, and 3) TUG test execution time for the impaired participants. The ground reaction forces in healthy and impaired participants did not show any significant differences. The compensatory gait patterns also showed inconsistent changes during treadmill walking. While a larger sample size is required to quantify the effects of the soft exosuit, this study provides some preliminary evidence on the potentials of the exosuit in assisting healthy individuals and stroke survivors.

A fourth version of the inflatable exosuit was designed keeping in mind, the drawbacks of the previous versions. The first through third versions of the exosuit utilized inflatable actuators with higher volumes limiting the use of the exosuit to indoor applications with a large pressure source. The design of a low volume inflatable actuator composite and a portable pneumatic source were presented. Finite element models

for the inflatable actuators and composites were generated and compared with experimental results. The composites were characterized for inflation speed, force output, and hysteresis. A portable pneumatic source capable of generating 0.131 MPa and 21.45 $SLPM$ was designed. A soft exosuit utilizing the inflatable actuator composites and the portable pneumatic source to assist knee extension was designed and applied to three healthy participants. Assistance during the stance phase of incline walking was provided and a reduction of the Vastus Lateralis muscle group was observed for all participants.

6.2 Future Work

Overall, this work presented the design, development, and evaluation of several versions of a soft inflatable exosuit for knee extension assistance. Future work for the exosuit should address the design of an additional degree of freedom for the knee joint in the form of knee flexion to completely assist the gait phase. With knee flexion assistance, stiffness control for the exosuit during the entire gait phase can be explored. Additionally, the soft actuators can be optimized to further design inflatable systems which can be taken outdoor and be used in a day-to-day applications. Furthermore, design of soft-inflatable actuators with varying geometries and shapes for wearable applications can be explored.

The design of a hip, knee, and ankle exosuit using inflatable actuators could be explored. Further user studies in different scenarios such as stair climbing and sit-to-stand transfers can be performed to investigate the feasibility of inflatable systems for use in wearable systems. Additionally, effective human intent detection and control methods to assist various physical activities can be explored as part of future work.

References

[1] A. Towfighi and J. L. Saver, "Stroke declines from third to fourth leading cause of death in the united states: historical perspective and challenges ahead," *Stroke*, pp. STROKEAHA–111, 2011.

[2] D. Mozaffarian, E. J. Benjamin, A. S. Go, D. K. Arnett, M. J. Blaha, M. Cushman, S. R. Das, S. de Ferranti, J.-P. Després, H. J. Fullerton *et al.*, "Heart disease and stroke statistics—2016 update: a report from the american heart association," *Circulation*, pp. CIR–0 000 000 000 000 350, 2015.

[3] P. Plummer, A. L. Behrman, P. W. Duncan, P. Spigel, D. Saracino, J. Martin, E. Fox, M. Thigpen, and S. A. Kautz, "Effects of Stroke Severity and Training Duration on Locomotor Recovery After Stroke: A Pilot Study," *Neurorehabilitation and Neural Repair*, vol. 21, no. 2, pp. 137–151, 2007.

[4] S. M. Lai, S. Studenski, P. W. Duncan, and S. Perera, "Persisting consequences of stroke measured by the stroke impact scale," *Stroke*, vol. 33, no. 7, pp. 1840–1844, 2002.

[5] F. Chantraine, C. Detrembleur, and T. M. Lejeune, "Effect of the rectus femoris motor branch block on post-stroke stiff-legged gait," *Acta Neurologica Belgica*, vol. 105, no. 3, p. 171, 2005.

[6] C.-L. Chen, H.-C. Chen, S. F.-T. Tang, C.-Y. Wu, P.-T. Cheng, and W.-H. Hong, "Gait performance with compensatory adaptations in stroke patients with different degrees of motor recovery," *American journal of physical medicine & rehabilitation*, vol. 82, no. 12, pp. 925–935, 2003.

[7] J. M. Ortman, V. A. Velkoff, H. Hogan *et al.*, *An aging nation: the older population in the United States.* United States Census Bureau, Economics and Statistics Administration, US . . . , 2014.

[8] K. C. Fleming, J. M. Evans, and D. S. Chutka, "Caregiver and clinician shortages in an aging nation," in *Mayo Clinic Proceedings*, vol. 78, no. 8. Elsevier, 2003, pp. 1026–1040.

[9] V. Lin, X. Zhang, and P. Dixon, "Occupational Therapy Workforce in the United States: Forecasting Nationwide Shortages," *PM and R*, vol. 7, no. 9, pp. 946–954, 2015. [Online]. Available: http://dx.doi.org/10.1016/j.pmrj.2015.02.012

[10] M. L. Aisen, H. I. Krebs, N. Hogan, F. McDowell, and B. T. Volpe, "The effect of robot-assisted therapy and rehabilitative training on motor recovery following stroke," *Archives of neurology*, vol. 54, no. 4, pp. 443–446, 1997.

[11] G. Kwakkel, B. J. Kollen, and H. I. Krebs, "Effects of robot-assisted therapy on upper limb recovery after stroke: a systematic review," *Neurorehabilitation and neural repair*, vol. 22, no. 2, pp. 111–121, 2008.

[12] B. Vanderborght, A. Albu-Schäffer, A. Bicchi, E. Burdet, D. G. Caldwell, R. Carloni, M. Catalano, O. Eiberger, W. Friedl, G. Ganesh *et al.*, "Variable impedance actuators: A review," *Robotics and autonomous systems*, vol. 61, no. 12, pp. 1601–1614, 2013.

[13] S. K. Banala, S. K. Agrawal, A. Fattah, V. Krishnamoorthy, W. L. Hsu, J. Scholz, and K. Rudolph, "Gravity-balancing leg orthosis and its performance evaluation," *IEEE Transactions on Robotics*, vol. 22, no. 6, pp. 1228–1239, 2006.

[14] A. J. Del-Ama, A. D. Koutsou, J. C. Moreno, A. De-los Reyes, A. Gil-Agudo, and J. L. Pons, "Review of hybrid exoskeletons to restore gait following spinal cord injury," *The Journal of Rehabilitation Research and Development*, vol. 49, no. 4, p. 497, 2012. [Online]. Available: http://www.rehab.research.va.gov/jour/2012/494/pdf/delama494.pdf

[15] W. Huo, S. Mohammed, J. C. Moreno, and Y. Amirat, "Lower limb wearable robots for assistance and rehabilitation: A state of the art," *IEEE systems Journal*, vol. 10, no. 3, pp. 1068–1081, 2016.

[16] S. Viteckova, P. Kutilek, and M. Jirina, "Wearable lower limb robotics: A review," *Biocybernetics and biomedical engineering*, vol. 33, no. 2, pp. 96–105, 2013.

[17] A. M. Dollar and H. Herr, "Lower extremity exoskeletons and active orthoses: challenges and state-of-the-art," *IEEE Transactions on robotics*, vol. 24, no. 1, pp. 144–158, 2008.

[18] M. F. Bruni, C. Melegari, M. C. De Cola, A. Bramanti, P. Bramanti, and R. S. Calabrò, "What does best evidence tell us about robotic gait rehabilitation in stroke patients: a systematic review and meta-analysis," *Journal of Clinical Neuroscience*, vol. 48, pp. 11–17, 2018.

[19] M. Grimmer, R. Riener, C. J. Walsh, and A. Seyfarth, "Mobility related physical and functional losses due to aging and disease-a motivation for lower limb exoskeletons," *Journal of neuroengineering and rehabilitation*, vol. 16, no. 1, p. 2, 2019.

[20] E. Guizzo and H. Goldstein, "The rise of the body bots [robotic exoskeletons]," *IEEE spectrum*, vol. 42, no. 10, pp. 50–56, 2005.

[21] G. Chen, C. K. Chan, Z. Guo, and H. Yu, "A review of lower extremity assistive robotic exoskeletons in rehabilitation therapy," *Critical Reviews^{TM} in Biomedical Engineering*, vol. 41, no. 4-5, 2013.

[22] M. K. Shepherd and E. J. Rouse, "Design and validation of a torque-controllable knee exoskeleton for sit-to-stand assistance," *IEEE/ASME Transactions on Mechatronics*, vol. 22, no. 4, pp. 1695–1704, 2017.

[23] M. Wehner, D. Rempel, and H. Kazerooni, "Lower extremity exoskeleton reduces back forces in lifting," in *ASME 2009 dynamic systems and control conference.* American Society of Mechanical Engineers, 2009, pp. 49–56.

[24] M. P. De Looze, T. Bosch, F. Krause, K. S. Stadler, and L. W. O'Sullivan, "Exoskeletons for industrial application and their potential effects on physical work load," *Ergonomics*, vol. 59, no. 5, pp. 671–681, 2016.

[25] R. Ranaweera, R. Gopura, T. Jayawardena, and G. K. Mann, "Development of a passively powered knee exoskeleton for squat lifting," *Journal of Robotics, Networking and Artificial Life*, vol. 5, no. 1, pp. 45–51, 2018.

[26] D. Zanotto, Y. Akiyama, P. Stegall, and S. K. Agrawal, "Knee joint misalignment in exoskeletons for the lower extremities: Effects on user's gait," *IEEE Transactions on Robotics*, vol. 31, no. 4, pp. 978–987, 2015.

[27] P. Polygerinos, N. Correll, S. A. Morin, B. Mosadegh, C. D. Onal, K. Petersen, M. Cianchetti, M. T. Tolley, and R. F. Shepherd, "Soft robotics: Review of fluid-driven intrinsically soft devices; manufacturing, sensing, control, and applications in human-robot interaction," *Advanced Engineering Materials*, vol. 19, no. 12, p. 1700016, 2017.

[28] Z. Wang, M. Z. Chen, and J. Yi, "Soft robotics for engineers," *HKIE Transactions*, vol. 22, no. 2, pp. 88–97, 2015.

[29] C. Laschi, B. Mazzolai, and M. Cianchetti, "Soft robotics: Technologies and systems pushing the boundaries of robot abilities," *Sci. Robot.*, vol. 1, no. 1, p. eaah3690, 2016.

[30] P. Boyraz, G. Runge, and A. Raatz, "An overview of novel actuators for soft robotics," in *Actuators*, vol. 7, no. 3. Multidisciplinary Digital Publishing Institute, 2018, p. 48.

[31] F. Daerden and D. Lefeber, "Pneumatic artificial muscles: actuators for robotics and automation," *European journal of mechanical and environmental engineering*, vol. 47, no. 1, pp. 11–21, 2002.

[32] K. C. Galloway, P. Polygerinos, C. J. Walsh, and R. J. Wood, "Mechanically programmable bend radius for fiber-reinforced soft actuators," in *Advanced Robotics (ICAR), 2013 16th International Conference on.* IEEE, 2013, pp. 1–6.

[33] E. H. Skorina, M. Luo, W. Y. Oo, W. Tao, F. Chen, S. Youssefian, N. Rahbar, and C. D. Onal, "Reverse pneumatic artificial muscles (rpams): Modeling, integration, and control," *PloS one*, vol. 13, no. 10, p. e0204637, 2018.

[34] S. Sridar, C. J. Majeika, P. Schaffer, M. Bowers, S. Ueda, A. J. Barth, J. L. Sorrells, J. T. Wu, T. R. Hunt, and M. Popovic, "Hydro muscle-a novel soft fluidic actuator," in *Robotics and Automation (ICRA), 2016 IEEE International Conference on.* IEEE, 2016, pp. 4014–4021.

[35] A. Miriyev, K. Stack, and H. Lipson, "Soft material for soft actuators," *Nature communications*, vol. 8, no. 1, p. 596, 2017.

[36] N. Kellaris, V. G. Venkata, G. M. Smith, S. K. Mitchell, and C. Keplinger, "Peano-hasel actuators: Muscle-mimetic, electrohydraulic transducers that linearly contract on activation," *Science Robotics*, vol. 3, no. 14, p. eaar3276, 2018.

[37] Y. Nishioka, M. Uesu, H. Tsuboi, and S. Kawamura, "Proposal of an extremely lightweight soft actuator using plastic films with a pleated structure," in *Mechatronics and Machine Vision in Practice (M2VIP), 2012 19th International Conference.* IEEE, 2012, pp. 474–479.

[38] C. Gosselin, "Cable-driven parallel mechanisms: state of the art and perspectives," *Mechanical Engineering Reviews*, vol. 1, no. 1, pp. DSM0004–DSM0004, 2014.

[39] M. Wehner, Y.-L. Park, C. Walsh, R. Nagpal, R. J. Wood, T. Moore, and E. Goldfield, "Experimental characterization of components for active soft orthotics," in *Biomedical Robotics and Biomechatronics (BioRob), 2012 4th IEEE RAS & EMBS International Conference on.* IEEE, 2012, pp. 1586–1592.

[40] L. N. Awad, J. Bae, K. O'donnell, S. M. De Rossi, K. Hendron, L. H. Sloot, P. Kudzia, S. Allen, K. G. Holt, T. D. Ellis *et al.*, "A soft robotic exosuit improves walking in patients after stroke," *Science translational medicine*, vol. 9, no. 400, p. eaai9084, 2017.

[41] L. N. Awad, J. Bae, P. Kudzia, A. Long, K. Hendron, K. G. Holt, K. O'donnell, T. D. Ellis, and C. J. Walsh, "Reducing circumduction and hip hiking during hemiparetic walking through targeted assistance of the paretic limb using a soft robotic exosuit," *American journal of physical medicine & rehabilitation*, vol. 96, no. 10, pp. S157–S164, 2017.

[42] P. M. Aubin, H. Sallum, C. Walsh, L. Stirling, and A. Correia, "A pediatric robotic thumb exoskeleton for at-home rehabilitation: The Isolated Orthosis for Thumb Actuation (IOTA)," *IEEE International Conference on Rehabilitation Robotics*, 2013.

[43] Y.-L. Park, B.-r. Chen, D. Young, L. Stirling, R. J. Wood, E. Goldfield, and R. Nagpal, "Bio-inspired active soft orthotic device for ankle foot pathologies," in *Intelligent Robots and Systems (IROS), 2011 IEEE/RSJ International Conference on.* IEEE, 2011, pp. 4488–4495.

[44] S. W. John, K. Murakami, M. Komatsu, and S. Adachi, "Cross-wire assist suit concept, for mobile and lightweight multiple degree of freedom hip assistance," in *Rehabilitation Robotics (ICORR), 2017 International Conference on.* IEEE, 2017, pp. 387–393.

[45] C. Thakur, K. Ogawa, T. Tsuji, and Y. Kurita, "Soft wearable augmented walking suit with pneumatic gel muscles and stance phase detection system to assist gait," *IEEE Robotics and Automation Letters*, vol. 3, no. 4, pp. 4257–4264, 2018.

[46] C. T. O'Neill, N. S. Phipps, L. Cappello, S. Paganoni, and C. J. Walsh, "A soft wearable robot for the shoulder: Design, characterization, and preliminary testing," in *Rehabilitation Robotics (ICORR), 2017 International Conference on.* IEEE, 2017, pp. 1672–1678.

[47] C. S. Simpson, A. M. Okamura, and E. W. Hawkes, "Exomuscle: An inflatable device for shoulder abduction support," in *Robotics and Automation (ICRA), 2017 IEEE International Conference on.* IEEE, 2017, pp. 6651–6657.

[48] H. Sareen, U. Umapathi, P. Shin, Y. Kakehi, J. Ou, H. Ishii, and P. Maes, "Printflatables: printing human-scale, functional and dynamic inflatable objects," in *Proceedings of the 2017 CHI Conference on Human Factors in Computing Systems.* ACM, 2017, pp. 3669–3680.

[49] C. M. Thalman, Q. P. Lam, P. H. Nguyen, S. Sridar, and P. Polygerinos, "A Novel Soft Elbow Exosuit to Supplement Bicep Lifting Capacity," in *2018 IEEE/RSJ International Conference on Intelligent Robots and Systems, IROS*, 2018, [Accepted].

[50] L. Cappello, J. T. Meyer, K. C. Galloway, J. D. Peisner, R. Granberry, D. A. Wagner, S. Engelhardt, S. Paganoni, and C. J. Walsh, "Assisting hand function after spinal cord injury with a fabric-based soft robotic glove," *Journal of neuroengineering and rehabilitation*, vol. 15, no. 1, p. 59, 2018.

[51] J. Chung, R. Heimgartner, C. T. O'Neill, N. S. Phipps, and C. J. Walsh, "Exoboot, a soft inflatable robotic boot to assist ankle during walking: Design, characterization and preliminary tests," in *2018 7th IEEE International Conference on Biomedical Robotics and Biomechatronics (Biorob).* IEEE, 2018, pp. 509–516.

[52] R. S. Diteesawat, T. Helps, M. Taghavi, and J. Rossiter, "High strength bubble artificial muscles for walking assistance," in *2018 IEEE International Conference on Soft Robotics (RoboSoft).* IEEE, 2018, pp. 388–393.

[53] P. R. Cavanagh and R. J. Gregor, "Knee joint torque during the swing phase of normal treadmill walking," *Journal of Biomechanics*, vol. 8, no. 5, pp. 339–344, 1975.

[54] J. M. Gere and S. Timoshenko, "Mechanics of materials, ; brooks," *Cole, Pacific Grove, CA*, pp. 815–39, 2001.

[55] W. Zhang, M. Tomizuka, and N. Byl, "A Wireless Human Motion Monitoring System for Smart Rehabilitation," *Journal of Dynamic Systems, Measurement, and Control*, vol. 138, no. 11, p. 111004, 2016. [Online]. Available: http://dynamicsystems.asmedigitalcollection.asme.org/article.aspx?doi=10.1115/1.4033949

[56] S. O. H. Madgwick, A. J. L. Harrison, and R. Vaidyanathan, "Estimation of IMU and MARG orientation using a gradient descent algorithm," in *2011 IEEE International Conference on Rehabilitation Robotics*, 2011, pp. 1–7. [Online]. Available: http://ieeexplore.ieee.org.ezproxy1.lib.asu.edu/ielx5/5961155/5975334/05975346.pdf?tp={&}arnumber=5975346{&}isnumber=5975334http://ieeexplore.ieee.org.ezproxy1.lib.asu.edu/abstract/document/5975346/?reload=true

[57] N. Karavas, A. Ajoudani, N. Tsagarakis, J. Saglia, A. Bicchi, and D. Caldwell, "Tele-Impedance based stiffness and motion augmentation for a knee exoskeleton device," in *2013 IEEE International Conference on Robotics and Automation*, 2013, pp. 2194–2200. [Online]. Available: http://ieeexplore.ieee.org.ezproxy1.lib.asu.edu/ielx7/6615630/6630547/06630872.pdf?tp={&}arnumber=6630872{&}isnumber=6630547http://ieeexplore.ieee.org.ezproxy1.lib.asu.edu/document/6630872/{#}full-text-section

[58] R. E. Kearney and I. W. Hunter, "System identification of human joint dynamics." *Critical reviews in biomedical engineering*, vol. 18, no. 1, pp. 55–87, 1990.

[59] R. Merletti and H. Hermens, "Introduction to the special issue on the SE-NIAM European Concerted Action," *Journal of Electromyography and Kinesiology*, vol. 10, no. 5, pp. 283–286, 2000.

[60] T. Venckunas, E. Trinkunas, S. Kamandulis, J. Poderys, A. Grunovas, and M. Brazaitis, "Effect of lower body compression garments on hemodynamics in response to running session," *Scientific World Journal*, vol. 2014, 2014.

[61] J. A. Faulkner, D. Gleadon, J. McLaren, and J. R. Jakeman, "Effect of Lower-Limb Compression Clothing on 400-m Sprint Performance," *Journal of Strength and Conditioning Research*, vol. 27, no. 3, pp. 669–676, 2013. [Online]. Available: http://content.wkhealth.com/linkback/openurl?sid=WKPTLP:landingpage{&}an=00124278-201303000-00016

[62] R. S. Snell, *Clinical anatomy by regions*. Lippincott Williams & Wilkins, 2011.

[63] S. Moore, K. Schurr, A. Wales, A. Moseley, and R. Herbert, "Observation and analysis of hemiplegic gait: swing phase," *Australian journal of physiotherapy*, vol. 39, no. 4, pp. 271–278, 1993.

[64] J. Perry, J. R. Davids *et al.*, "Gait analysis: normal and pathological function," *Journal of Pediatric Orthopaedics*, vol. 12, no. 6, p. 815, 1992.

[65] C. M. Thalman, Q. P. Lam, P. H. Nguyen, S. Sridar, and P. Polygerinos, "A novel soft elbow exosuit to supplement bicep lifting capacity," in *International Conference on Intelligent Robots and Systems (IROS)*. IEEE, 2018, pp. 6965–6971.

[66] S. Sridar, P. H. Nguyen, M. Zhu, Q. P. Lam, and P. Polygerinos, "Development of a soft-inflatable exosuit for knee rehabilitation," in *Intelligent Robots and Systems (IROS), 2017 IEEE/RSJ International Conference on*. IEEE, 2017, pp. 3722–3727.

[67] S. Sridar, Z. Qiao, N. Muthukrishnan, W. Zhang, and P. P. Polygerinos, "A soft-inflatable exosuit for knee rehabilitation: Assisting swing phase during walking," *Frontiers in Robotics and AI*, vol. 5, p. 44, 2018.

[68] P. T. Chinimilli, S. W. Wachtel, P. Polygerinos, and W. Zhang, "Hysteresis compensation for ground contact force measurement with shoe-embedded air pressure sensors," in *ASME 2016 Dynamic Systems and Control Conference*. American Society of Mechanical Engineers, 2016, pp. V001T09A006–V001T09A006.

[69] J. M. Gregson, M. Leathley, A. P. Moore, A. K. Sharma, T. L. Smith, and C. L. Watkins, "Reliability of the tone assessment scale and the modified ashworth scale as clinical tools for assessing poststroke spasticity," *Archives of physical medicine and rehabilitation*, vol. 80, no. 9, pp. 1013–1016, 1999.

[70] P. Greene and M. Granat, "The effects of knee and ankle flexion on ground clearance in paraplegic gait," *Clinical Biomechanics*, vol. 15, no. 7, pp. 536–540, 2000.

[71] B. Balaban and F. Tok, "Gait disturbances in patients with stroke," *PM&R*, vol. 6, no. 7, pp. 635–642, 2014.

[72] C. L. Lysack, "Household and neighborhood safety, mobility," in *Handbook of Assessment in Clinical Gerontology*. Elsevier, 2010, pp. 619–646.

[73] U.-B. Flansbjer, A. M. Holmbäck, D. Downham, C. Patten, and J. Lexell, "Reliability of gait performance tests in men and women with hemiparesis after stroke." *Journal of rehabilitation medicine*, vol. 37, no. 2, pp. 75–82, 2005.

[74] H.-T. D. Chun, J. O. Roberts, M. E. Sayed, S. Aracri, and A. A. Stokes, "Towards more energy efficient pneumatic soft actuators using a port-hamiltonian approach," in *2019 2nd IEEE International Conference on Soft Robotics (RoboSoft)*. IEEE, 2019, pp. 277–282.

[75] S. Veldman, O. Bergsma, and A. Beukers, "Bending of anisotropic inflated cylindrical beams," *Thin-walled structures*, vol. 43, no. 3, pp. 461–475, 2005.

[76] C. R. Nesler, T. A. Swift, and E. J. Rouse, "Initial design and experimental evaluation of a pneumatic interference actuator," *Soft robotics*, vol. 5, no. 2, pp. 138–148, 2018.

[77] J. Realmuto and T. Sanger, "A robotic forearm orthosis using soft fabric-based helical actuators," in *2019 2nd IEEE International Conference on Soft Robotics (RoboSoft)*. IEEE, 2019, pp. 591–596.

[78] W. G. Davids, "Finite-element analysis of tubular fabric beams including pressure effects and local fabric wrinkling," *Finite Elements in Analysis and Design*, vol. 44, no. 1-2, pp. 24–33, 2007.

[79] S. J. Kim, H. Chang, J. Park, and J. Kim, "Design of a portable pneumatic power source with high output pressure for wearable robotic applications," *IEEE Robotics and Automation Letters*, vol. 3, no. 4, pp. 4351–4358, 2018.

[80] "Topsflo tm40a-a," *TOPSFLO, www.topsflo.com.*

[81] "Knf nmp 850," *KNF Neuberger Inc., www.knfusa.com.*

[82] "Parker btx-connect," *Parker Hannifin, www.parker.com.*

[83] "Binaca gx-2," *Binaca Pumps, www.binacapumps.com.*

[84] W. Zhang, M. Tomizuka, and N. Byl, "A wireless human motion monitoring system for smart rehabilitation," *Journal of Dynamic Systems, Measurement, and Control*, vol. 138, no. 11, p. 111004, 2016.

[85] P. T. Chinimilli, S. Redkar, and W. Zhang, "Human activity recognition using inertial measurement units and smart shoes," in *2017 American Control Conference (ACC).* IEEE, 2017, pp. 1462–1467.